# CEBAF Program Advisory Committee Six (PAC6) Proposal Cover Sheet

This proposal must be received by close of business on April 5, 1993 at:

CEBAF
User Liaison Office
12000 Jefferson Avenue
Newport News, VA 23606

## Proposal Title

MEASUREMENT OF THE POLARIZATION OF THE $\phi(1020)$ IN ELECTROPRODUCTION

## Contact Person


**Name:** ELTON SMITH
**Institution:** CEBAF, PHYSICS DIV
**Address:** 12,000 JEFFERSON AVE.
**Address:**
**City, State ZIP/Country:** NEWPORT NEWS, VA 23693
**Phone:** (804) 249-7625 **FAX:** (804) 249-5800
**E-Mail → BITnet:** ELTON @ CEBAF **Internet:** ELTON @ CEBAF2.CEBAF.GOV


**If this proposal is based on a previously submitted proposal or letter-of-intent, give the number, title and date:**

**CEBAF Use Only**

Receipt Date: 4/5/93 Log Number Assigned: PR 93-022

By: gp

# Measurement of the Polarization of the $\phi(1020)$ in Electroproduction

W.K. Brooks, V. Burkert, B. Mecking, M.D. Mestayer, B. Niczyporuk, E. S. Smith, A.Yegneswaran
*CEBAF, Newport News, Virginia*

L. Dennis, P. Dragovitsch, A. Williams
*Florida State University, Tallahassee, Florida*

K. Baker, K. Beard
*Hampton University, Hampton, Virginia*

M. Kossov
*ITEP, Moskow, Russia*

A. Tam
*University of South Carolina, Columbia, South Carolina*

J. Ficenec, D. Jenkins
*Virginia Polytechnic Institute and State University, Blacksburg, Virginia*

A. Coleman, M. Eckhause, H. Funsten, J. Kane, P. Rubin, T. Tung, R. Welsh
*College of William and Mary, Williamsburg, Virginia*

and the CLAS

STRUCTURE OF THE NUCLEON PHYSICS WORKING GROUP

Spokespersons: H. Funsten, P. Rubin and E.S. Smith

**Abstract**

We propose to measure the reaction $e^- p \rightarrow e^- p \phi$ at a beam energy of 4 GeV. The polarization of the $\phi$ meson will be determined from the angular correlations in the decay $\phi \rightarrow K^+K^-$. We expect adequate statistical sensitivity in the decay distribution to determine the components due to longitudinal and transverse scattering to about 10%. The same sensitivity allows us to measure the fraction of $\phi$ production due to pseudoscalar exchange mechanisms relative to diffractive scattering. An enhancement in this component may indicate a significant strangeness content in the proton.

# 1 Overview

Vector meson production has been an important tool used in understanding the hadronic properties of the photon [1]. For low values of $Q^2$ and W, the photon interacts with the target predominately through vector meson intermediate states which diffractively scatter from the target, conserving helicity, a process called Vector-Meson Dominance (VMD). However, as was first discovered in the mid 1970's, for larger values of $Q^2$, the photon directly probes the constituents in the nucleon. This experiment proposes polarization measurements of $\phi$ electroproduction in the transition region.

Electromagnetic production of $\phi$ mesons is simple relative to other vector mesons because its valence quark structure is pure $s\bar{s}$ (see Appendix A). Unlike the case for $\omega$ or $\rho$ production, quark exchange diagrams are inhibited. These OZI suppressions occur at a level between 0.1 - 5% of OZI allowed reactions. (For example, $\Gamma_{\phi \rightarrow \rho\pi} \approx 0.6$ MeV, less than 0.6% of typical hadronic widths). Measurement of a $\phi$ electroproduction component arising from a $\phi$-N interaction significantly greater than the 5% expected from OZI violation could be indicative of an $s\bar{s}$ component in the nucleon.

Figure 1 sketches kinematic quantities of interest in the electroproduction of $\phi$ mesons. The relatively high luminosity attainable at CEBAF and the large acceptance of the CLAS detector will allow the study of the angular distributions of K mesons from $\phi$ decay, which up to now have only been inferred from models, for the helicity-conserving diffractive and pseudoscalar exchange mechanisms.

## 1.1 Hard Production Mechanisms

Measurements at high $Q^2$ show that there are kinematic regions where exclusive production of vector mesons is a hard scattering process. The EMC Collaboration [3] has measured exclusive $\rho$ vector meson production with muons, i.e. $\mu p \rightarrow \mu \rho^o p$. Their data indicate that in this regime, the soft hadron-like properties of the photon have disappeared and the (virtual) photon acts as pure electromagnetic probe of the nucleon structure. A signature for the departure from the diffractive nature of the reaction mechanism is given by $\rho^o \rightarrow \pi^+\pi^-$ decay distribution shown in Figure 2. A pure longitudinal cross section, i.e. a $\cos^2\theta$ distribution, is unexpectedly observed. Their analysis suggests that hard production mechanisms in exclusive muoproduction are present at $Q^2 \gtrsim 1$ GeV$^2$. Exclusive $\rho$ production measurements at lower energies have the same trend [2].

Inclusive $\phi$ photoproduction measurements [4] for photon energies between 20 and 70 GeV also show that the $\phi$ angular decay distribution is a sensitive measure of the onset of non-diffractive production mechanisms. The diffractive character of the reaction mechanism is reflected in the $\sin^2\theta$ distribution in Figure 2 for $x_F \geq 0.7$, where $x_F$ is the momentum of the vector meson along the photon beam relative to the maximum allowed in the center-of-mass. Hard processes, described within the quark fusion model, are indicated by a very different angular distribution for $0.1 \leq x_F \leq 0.7$. Interpreted as the onset of hard photoknockout of a $s\bar{s}$ pair, the data suggest about a 20 - 30 % $s\bar{s}$ nucleon component (see Section 1.2 below).

The lack of substantial $\phi$-nucleon coupling makes it a useful indicator of the onset of hard processes. However, no previous electroproduction experiment has accumulated enough data to measure $\phi$ decay angular distributions with the accuracy required to indicate this onset.

We intend to measure the $\phi$ polarization observables in exclusive production at $Q^2$ between 0.3 and 2 GeV$^2$. In particular, we expect to measure the decay distributions as a function of the azimuthal angle, which has not been possible for the higher energy experiments. The complete angular coverage of the CLAS detector allows independent determinations of longitudinal and transverse scattering to about 10 %. Such measurements may allow us to identify hard production mechanisms if they exist in this kinematic region.

## 1.2 $\phi$ Production by $s\bar{s}$ Knockout

A number of unexpected experimental results may be explained by assuming that the nucleon $s\bar{s}$ sea component is of the order 10-20% [9, 10]: 1) results from deep inelastic scattering of polarized muons on polarized protons [3]; 2) $\nu$p elastic scattering [5]; 3) the $\pi$-nucleon $\sigma$ term, obtained by extrapolating low energy $\pi$-N scattering to the unphysical pion pole [6, 7, 8]; 4) OZI suppressed reactions are at least a factor of 3 more than expected in $p\bar{p}$ annihilation: $(p\bar{p} \rightarrow \phi\pi^+\pi^-)/(p\bar{p} \rightarrow \omega\pi^+\pi^-) = 2-3\%$ compared to theoretical expectations of 0.1 - 0.7% [11]; 5) fits to the isoscalar Dirac nucleon electromagnetic form factor have to incorporate a $\phi$ vector meson component with a large nucleon coupling: $g_1(\phi NN)/g_1(\omega NN) \sim 0.4$ [12].

Several experiments have been proposed at CEBAF to measure strange quark effects in the proton at low $Q^2$ by using parity-violation in electron scattering [13, 14, 15]. However, these experiments are challenging and restricted to a very narrow range in $Q^2$.

An independent indicator of the nucleon's $s\bar{s}$ component is $\phi$ electroproduction. Schematically this process is shown in Figure 3. The rate of $\phi$ electromagnetic production on a nucleon via photon scattering from a virtual $s\bar{s}$ pair in the proton has been estimated in References [16, 17, 18]. The calculations indicate that the knockout and diffractive contributions to $\phi$ production are of the same magnitude when one assumes an admixture of 10–20% strange quarks in the nucleon (see Figure 4). The calculations assume the $s\bar{s}$ pair to be in a relative 1s-state with respect to each other inside the proton just as they are in the $\phi$. The spin of the $s\bar{s}$ pair is taken to be either 0 or 1. However, only the spin zero component survives because of cancellations between $\gamma_v\bar{s}$-quark and $\gamma_v s$-quark contributions. Spin 0 is also expected from C-conjugation and hyperfine-splitting arguments. The parity of the pair is negative, since the intrinsic parity of the $s$-quark is opposite to that of the $\bar{s}$-quark. Thus, $\phi$ production due to $s\bar{s}$ knockout proceeds through the exchange of a pseudoscalar in the t-channel.

Pseudoscalar exchange provides a particularly simple signal in the $\phi \rightarrow K^+K^-$ decay distribution if evaluated in the Gottfried-Jackson frame (see Appendix B):

$$W^{GJ}_{PS}(\cos\theta,\psi) = \frac{3}{8\pi}\sin^2\theta\,(1 + P_\sigma\,\epsilon\cos 2\psi) \qquad (1)$$

The angle $\theta$ is the polar angle of the $K^+$ and $\psi$ is the azimuthal angle

relative to the electron scattering plane (*not* the hadron production plane). Because a spin 0 object is exchanged, the polarization of the $\phi$ cannot depend on the orientation of the hadron production plane. Furthermore, the $\phi$ has no longitudinal spin component. The $\sin^2\theta$ term arises from $\phi$'s polarized in the $\pm 1$ helicity state. The $\cos 2\psi$ term is due to interference between the two transverse helicity states. For pseudoscalar meson exchange (unnatural parity), $P_\sigma = -1$; for the case of diffraction (natural parity), $P_\sigma = +1$. The $\cos 2\psi$ term, a key to identifying pseudoscalar meson exchange, is proportional to the transverse linear polarization of the photon, either real or virtual. In the helicity frame the distribution in Equation 1 is modified in a predictable way as a function of the momentum transfer t, as given in the Appendix B, and yields a second key to identifying pseudoscalar exchange.

# 2 Sources of $K^+K^-$ Pairs

The production of $K^+K^-$ pairs may proceed through various channels in addition to $s\bar{s}$ knockout, described above. These include

- Diffractive production of $\phi$'s.
- t - channel exchange of $\pi$ and $\eta$ mesons.
- Associated production of high mass strange baryons.

We must be able to isolate our signal from these background reactions, which are illustrated Figure 5. In the sections below we will review each reaction in turn. Diffraction is the dominant production mechanism of $\phi$'s. However, it can be distinguished from pseudoscalar meson exchange by its significantly different decay angular distribution. Excited strange baryons are kinematically distinct and we use the particle identification and missing mass resolution of the CLAS to remove these events from our sample. Finally the production of $\phi$'s due to the exchange of pions and etas is an intrinsic background, but the rate due to this mechanism is calculable and small.

## 2.1 Diffractive Production

The dominant mechanism for $\phi$ production at low momentum transfer is diffraction, which is analyzed using Vector-Meson Dominance (VMD). Refer

to Appendices B and C for details. Within this framework, the polarization of $\phi$'s is the same as the polarization of the virtual photon in the helicity frame, a mechanism refered to as s-channel Helicity Conservation (SCHC). Under these assumptions [21], the decay distribution $W_D(\cos\theta,\psi)$ of the $K^+$ in the rest frame of the $\phi$ has the same form as Equation 1, but with additional terms due to longitudinal and longitudinal-transverse polarizations:

$$\begin{aligned} W_D(\cos\theta,\psi) &= \frac{3}{8\pi}\left(\frac{1}{1+\epsilon R}\right)\{\sin^2\theta\,(1+\epsilon\cos 2\psi) \\ &\quad + 2\epsilon R\cos^2\theta \\ &\quad - \sqrt{2\epsilon(1+\epsilon)R}\cos\delta\,\sin 2\theta\,\cos\psi\} \end{aligned} \tag{2}$$

Here $\sqrt{R}e^{i\delta}$ is the ratio of longitudinal to transverse amplitudes. The term proportional to $\cos^2\theta$ is due to longitudinal $\phi$'s, that is, helicity zero. We make particular note that $W_D(\cos\theta,\psi)$, evaluated in the helicity frame, is independent of the momentum-transfer t. If VMD applies, R scales [19] as

$$R = \xi^2\frac{Q^2}{M_\phi^2} \tag{3}$$

As noted in Section 1.1, the increase in R with $Q^2$ predicted by Equation 3 was confirmed in leptoproduced $\rho$ decay distribution measurements. However, the cross section measurements disagree, and show that R is consistent with zero. Hard scattering measurements of the $W_1$ and $W_2$ proton structure functions in the deep inelastic region also show that R is small ($\sim$0.13) and does not scale with $Q^2$ as in Equation 3 [1].

The proposed CLAS experiment will be able to determine the diffractive components in the decay correlation, i.e., R and $\cos\delta$, to within 10% for $Q^2$ ranging between 0.3 and 2 GeV$^2$.

## 2.2 Strange Baryon Resonances

Associated electroproduction of high mass strange baryons which subsequently decay into a p $K^-$ pair is another mechanism for the production of $K^+K^-$. For example,

$$\begin{array}{l} \gamma_v\, p \rightarrow K^+\,\Lambda^* \\ \qquad\qquad\quad \hookrightarrow\; p\,K^- \end{array} \tag{4}$$

This reaction is kinematically distinct from $\phi$ production, as the invariant mass of the ($K^+K^-$) pair does not necessarily reconstruct to the $\phi$ mass. The backgrounds due to these resonances will be removed by a ($K^+K^-$) invariant mass cut as described in Section 4.

The electroproduction cross section for $\Lambda^*(1520)$ production is the same as for the production of $\phi$'s [20]. We assume in our simulations that the $\Lambda^*(1520)$, $\Lambda^*(1600)$ and $\Lambda^*(1670)$ are produced with equal cross section. The contamination of the sample is a strong function of the hadronic missing mass W (see Figure 6). At threshold, only the $\Lambda^*(1520)$ contributes. At W=2.5 $GeV^2$, none of the resonances are a background. For intermediate cases, each of the resonances may fall under the $\phi$ invariant mass peak. In the worst case, the sum of all three resonances may contribute as much as 10% to the cross section. However, these events may be reduced to 3% by accepting a 15% loss of efficiency of the $\phi$ sample (see Table 1).

## 2.3 $\pi$ and $\eta$ Exchange

$\phi$ production by t-channel exchange of $\pi$ and $\eta$ mesons is coherent with pseudoscalar ($s\bar{s}$) knockout and ultimately limits the sensitivity of this method. However, the production rate through this mechanism is small (~5% of the diffractive). The rates for these backgrounds were estimated from measured $\pi^o$ exchange contributions to $\omega$ photoproduction [1] scaled by known decay widths and appropriate coupling constants [23] (see Figure 7). An independent calculation using the electroproduction model of Fraas [24] shows that these estimates are conservative. The t-dependence of the reaction was assumed to be of the form

$$\sigma_{ps} \sim \frac{e^{1.6t}\, t}{(t - M_{ps}^2)^2} \tag{5}$$

where $M_{ps}$ is the mass of the pseudoscalar ($\pi$ of $\eta$) and t is the momentum transfer, which is negative. The exponential is an empirical representation of hadronic form factors [25]. The t in the numerator is required by parity and angular momentum conservation. The denominator is given by the meson propagator. The relative cross sections due to these reactions are shown in Figure 8. At low momentum transfer, the $\pi$ exchange diagram is dominant.

[1] See, for example, Reference [1] p. 330.

At larger t, the $\pi$ and $\eta$ diagrams become comparable. However the negative interference between these two amplitudes [2] was not included in the estimates, so the actual rate due to these backgrounds should be even smaller than calculated.

# 3 Previous Measurements

Most of the measurements of $\phi$ production have been realized in experiments with unpolarized real photons [26, 27, 28]. They indicate that the $\phi$'s are diffractively produced and conserve helicity. Their agreement with the predictions of the Vector Meson Dominance model was considered a confirmation of the model [29, 30]. However, these experiments are limited to $Q^2$=0 and are relatively insensitive to various production mechanisms due to their lack of polarization.

There is very little data of $\phi$ production with linearly polarized photons [31, 32]. Although the results were in general agreement with Vector Meson Dominance, the measured value of one density matrix, $\rho^1_{1-1}$ was notably low, $\approx 0.18 \pm .13$ compared to an expected value of 0.5. Within the quoted error bars, the values of $\rho^2_{1-1}$ and $\rho^1_{1-1}$ could indicate a pseudoscalar exchange cross section component as large as $\sim$ 30 % of the total.

There are only a few measurements of $\phi$ production by virtual photons. The parameters of the diffractive cross section (Table 6) were measured with two magnetic spectrometers [33], one detecting the electron, the other measuring the two charged kaons from the decay of the $\phi$. Data were taken at $Q^2$= 0.23, 0.43 and 0.97 GeV$^2$. Their decay distributions, together with the fitted distributions are shown in Figure 9. The LAME experiment [2] extended the cross section measurements to higher $Q^2$= 0.8–4 GeV$^2$ and covered a range in W between 2 and 3.7 GeV. Their measurements confirmed the parameters in Table 6, but did not constrain them further. Finally there is a very low statistics experiment measuring $\phi$ production by muons [34]. All experimental results generally agree with the expectations of the VMD model for $\phi$ production. However, the sensitivity of the measurements was quite limited, and the model, which contains several parameters, is able to accommodate a broad range of results.

[2] See Reference [30] p. 908.

Table 2 is a summary of existing measurements which may be used to place limits on the the fraction $f_{PS}$ of the data arising from pseudoscalar exchange.

# 4 Simulation of the Experiment

The process we wish to study is $e^-p \rightarrow e^-p\phi$, with the $\phi$ decaying into $K^+K^-$ (see Figure 10). The identification of the electron and proton is sufficient to identify $\phi$ production by the missing mass technique. However, the polarization measurement of the $\phi$ demands the detection of a third particle. We require, then, the detection of the electron and any pair of the p, $K^+$ and $K^-$.

In order to optimize our physics goals, we choose to run with the beam energy set at 4 GeV and the CLAS magnetic field set at half the nominal field with negative particles bending toward the axis. The kinematic boundaries for the acceptance of the electron in this configuration of the CLAS detector are shown in Figure 11. To determine the acceptance of the detector and estimate the $\phi$ production rate, we have written an event generator which simulated diffractive $\phi$ production according to Equation 10 (see Appendix C). The Monte Carlo generated events were then processed with FASTMC [35], which models the acceptance and resolution of the CLAS detector. Events were generated at fixed values of $Q^2$ and W to determine the acceptance for various kinematics. The calculated acceptance in ($Q^2$,W) bins is given in Table 4. The corresponding number of $\phi$'s expected during a 350-hour run is given Table 5. We expect about 22,000 $\phi$ events integrated over all kinematic quantities during this period.

To study the response of the detector in greater detail, we picked a region in $Q^2$ and W which corresponds to one of several kinematic regions which we would use for the decay angular distribution analysis. This region was constrained to have relatively constant virtual photon polarization between $0.6 \leq \epsilon \leq 0.7$. For a 4 GeV beam, this region spans 0.4 $GeV^2 \leq Q^2 \leq 1.2$ $GeV^2$ and 2.0 GeV $\leq W \leq$ 2.3. After all analysis cuts (see below), we expect 4000 analyzable $\phi$ events in a 350-hour run in this ($Q^2$,W) region.

We have generated and analyzed through the FASTMC some 10,000 events with these parameters. The highest detection efficiency included the scattered electron, the scattered proton, and one of the kaons (see Table 3).

We reconstruct from these tracks the three-momentum of the other track, assuming it to be a kaon, and thereby the four-momentum of the $\phi$. The invariant mass reconstructed by this technique yields a resolution of about 7.5 MeV (see Figure 12), and we choose for further consideration those events for which this mass lies within $2.5\sigma$ of the nominal $\phi$ mass. Typically, the $K^-$ bends through the beam-pipe opening in the detector (see Figure 10), and we find that three quarters of our accepted events contain a well-measured $K^+$. Unfortunately, the same final state arises from electroproduced $K^+$ $\Lambda^*$s, where the $\Lambda^*$ decays to $K^-$ p (see Section 2.2). Events with higher mass $\Lambda^*$s reflect into $\phi$ mass region (see Figure 6). We minimize this background by reconstructing the $\Lambda^*$ and cutting on the invariant mass. The loss in $\phi$ efficiency may be as large as 15% at W=2.2 $GeV^2$ (see Table 1) to reduce the $\Lambda^*$ backgrounds to less than 3%. The efficiency for this procedure, except for cuts on $\Lambda^*$ invariant mass, is about 11% (see Table 4), reducing the number of analyzable $\phi$ events to 4000 in a 350-hour run.

Figure 14 shows the momentum spectrum of the kaons, which peaks at 1 GeV and with no entries above 1.4 GeV. This is well within the time-of-flight particle identification capabilities of CLAS. Figures 15 shows that the acceptance is smooth over all measured variables. In particular the decay angle of the $K^+$ can be reconstructed over the entire phase space in the $\phi$ rest frame (see Figure 13).

# 5 Angular Correlations

The $\phi(1020)$ is a spin 1 object. Its decay into $K^+K^-$, two spin-0 mesons, is "self-analyzing": the angular distributions provide a complete description of the $\phi$ polarization. The choice of coordinates, characteristic of each production mechanism, makes this polarization easily analyzable. We are interested, then, in measuring the decay angles of an identified kaon in the $\phi$ rest frame. These are the polar angle $\theta$ $(0 < \theta < \pi)$, the azimuthal angle $\varphi$ $(0 < \varphi < 2\pi)$, and $\Phi$, the angle between the electron scattering plane and the hadron production planes. We note that in Equations 1 and 2, and subsequently, $\psi = \Phi - \varphi$.

The helicity frame simplifies the description of diffractive scattering (Equation 2), so we have chosen this frame for the analysis. The appropriate reference frame for pseudoscalar t-exchange mechanisms is the Gottfried-Jackson

system. The decay distributions for pseudoscalar exchange are obtained in the helicity frame by rotating the density matrix elements by the angle $-\alpha_{H\to GJ}$. A description of these frames and the transformation between them is given in Appendix B.

Our objective is to measure angular components in the helicity frame which then can be attributed to pseudoscalar exchange. The signal for the pseudoscalar exchange mechanism, $W^H_{PS}(\cos\theta,\psi,\Phi;Q^2,W,t)$, will appear in the helicity frame as a predictable function of momentum transfer through its dependence on $\alpha_{H\to GJ}$. Since pseudoscalar exchange is incoherent with helicity-conserving diffraction [22], the decay distribution $W(\cos\theta,\psi,\Phi)$ is a linear combination of pseudoscalar exchange and diffraction with relative fractions $f_{PS}$ and $f_D$ respectively:

$$\begin{aligned} W(\cos\theta,\psi,\Phi) &= f_{PS}\, W^H_{PS}(\cos\theta,\psi,\Phi;Q^2,W,t) \\ &\quad + f_D\, W_D(\cos\theta,\psi;Q^2,\xi^2,\cos\delta) \end{aligned} \tag{6}$$

In the above equation we have explicitly shown the dependencies on the kinematic variables ($Q^2$, W and t) and parameters of the model ($\xi^2$, $\cos\delta$). The distributions for pure pseudoscalar exchange and pure diffractive production are shown separately in Figure 16. A multipole moment analysis with respect to these angles permits determination of combinations of the matrix elements.

## 5.1 Sensitivity

To estimate our sensitivity to various components of the distribution, we proceeded as follows: We choose a region in $Q^2$ and W containing 4000 useful $\phi$ events as described in Section 4. (There are five or six such regions for the experiment.) These events were selected further into four momentum transfer bins (see Equation 11), containing 2030, 1083, 578 and 308 events respectively. We then performed the following analysis. The angular distribution $W(\cos\theta,\psi,\Phi)$ was generated with the appropriate number of events in the three variables $\cos\theta$ and $\varphi$ and $\Phi$ using the values of the four parameters $f_{PS}$=15%, $f_D$=85%, and $\xi^2$ and $\cos\delta$ as given in Table 6. The angular distribution $W(\cos\theta,\psi,\Phi)$ was then fit [3] for the four parameters. Figure 17 shows the fitted angular distributions for t=–0.3 $GeV^2/c^2$ projected onto two

[3] We used HBOOK package to call the routines from MINUIT.

of the axes. We note that the full sensitivity of our analysis is partially lost by integration. However, this is the simplest way of comparing simulated data with the fitted curves.

The expected sensitivity as function of t is given in Figures 18 and 19. When the event sample is large, the parameters are determined as generated. However, when the sample is small (large t), we observe systematic shifts from the generated values. The "errors" plotted in the Figures include both statistical errors and systematic uncertainties in the fitting procedure. For small values of t, we can determine the pseudoscalar fraction to about 5%. At larger values of t, the sensitivity decreases to 10%. This sensitivity is at about the level of the average contribution of $\pi$ and $\eta$ exchange mechanisms to the production. The values of $\xi^2$ and $\cos\delta$, which determine the longitudinal and longitudinal-transverse components, can be determined to about 10%.

# 6 Summary

Sensitivities at the level of ~5–10% to the electroproduction of $\phi$ vector mesons due to mechanisms other than diffraction are achievable with 350 hours of beam time. This is possible due to a hundred-fold increase in the number of analyzable $\phi$ events over previous experiments and due to the large and uniform acceptance of the CLAS detector. To complete this measurement we request the following running conditions:

- Electron Beam Energy = 4 GeV.
- Proton Target.
- Luminosity = $10^{34}\text{cm}^{-2}\text{s}^{-1}$.
- 350 Hours of CLAS operation.
- Magnetic field set at half maximum with negative particles bending toward the axis.

# A Properties of the $\phi(1020)$

For completeness we review the properties of the $\phi(1020)$ meson [37]. The $\phi$ is a the vector meson ($J^{PC} = 1^{-}\ ^{-}$, I=0), with a mass of 1019.413±0.008 MeV and a full width $\Gamma$=4.43±0.06 MeV. The branching ratio for B($\phi \rightarrow K\ \overline{K}$) = 83.5%, with the fraction to charged kaons B($\phi \rightarrow K^{+}\ K^{-}$) = 49.1%. The only other significant branching fraction is B($\phi \rightarrow \rho\ \pi$) = 12.9%. The present experiment intends to make use of the decay to two charged kaons to tag the production of $\phi$'s.

Within the Quark Model for mesons, the $\phi$ may be written as a linear combination

$$|\phi\rangle \ = \ \cos\theta\ |s\bar{s}\rangle + \sin\theta\ \frac{1}{\sqrt{2}}|u\bar{u} + d\bar{d}\rangle \qquad (7)$$

where $\cos^2\theta$ represents the strange content in the $\phi$. Normally, the mixing is given in the context of SU(3) in terms of octet and singlet components with a mixing angle $\theta_v$. In terms of the SU(3) mixing angle, we can write

$$\cos\theta \ = \ \frac{\cos\theta_v}{\sqrt{3}}(\sqrt{2} \ + \ \tan\theta_v) \qquad (8)$$

Various estimates of the mixing angle allow for deviations of up to 4° from "ideal mixing," which corresponds to $\theta_v = 35.3°$. This determines the non-strange components in the $\phi$ to be less than 0.5%.

# B Decay Distributions

The $\phi \rightarrow K^+ K^-$ decay correlation, $W(cos\theta, \phi, \Phi)$, is the product of trigonometric functions of the $K^+ K^-$ decay angles, taken in the $\phi$ cm ($K^+$ and $K^-$ are back to back), and density matrix elements, $\rho_{\lambda,\lambda'}$, characterizing the $\phi$'s polarization. $\theta$ and $\phi$ are the polar and azimuthal decay angles and $\Phi$ is the angle between the electron and hadron scattering planes. Since $J_\gamma = J_\phi = 1$, the multipolarity in these angles = 2. Schilling and Wolfe [21] decompose $\rho_{\lambda,\lambda'}$ into components $\rho^\alpha_{\lambda,\lambda'}$ characteristic of the $\gamma_V$ polarization, i.e., $\alpha$ = 1, 2, ...6 = T, TT, TT, L, LT, LT. L = longitudinal, T = transverse. TT = transverse - transverse interference, etc. A general expression for W for electroproduced vector mesons is then derived in Reference [21] for unpolarized incident electrons:

$$
\begin{aligned}
W^{\text{unpol}}(\cos\theta, \phi, \Phi) &= \frac{1}{1+(\epsilon+\delta)R}\frac{3}{4\pi} \\
&\times [\tfrac{1}{2}(1-\rho^0_{00}) + \tfrac{1}{2}(3\rho^0_{00}-1)\cos^2\theta \quad -\sqrt{2}\ \text{Re}\ \rho^0_{10}\sin 2\theta\ \cos\phi \quad -\rho^0_{1-1}\sin^2\theta\cos 2\phi \\
&- \epsilon\cos 2\Phi\{\rho^1_{11}\sin^2\theta + \rho^1_{00}\cos^2\theta - \quad \sqrt{2}\ \text{Re}\ \rho^0_{10}\ \sin 2\theta\ \cos\phi \quad -\rho^1_{1-1}\sin^2\theta\cos 2\phi\} \\
&- \epsilon\sin 2\Phi\ \{\sqrt{2}\ \text{Im}\ \rho^2_{10}\sin 2\theta\ \sin\phi \quad +\text{Im}\ \rho^2_{1-1}\sin^2\theta\ \sin 2\phi\} \\
&+ (\epsilon+\delta)R\{\tfrac{1}{2}(1-\rho^4_{00} + \tfrac{1}{2}(3\rho^4_{00} - \quad 1)\cos^2\theta - \sqrt{2}\{\text{Re}\ \rho^4_{10}\sin \quad 2\theta\cos\phi \\
&\quad -\rho^4_{1-1}\sin^2\theta\cos 2\phi\} \\
&\quad + \sqrt{2\epsilon R(1+\epsilon+2\delta)}\cos\Phi\{\rho^5_{11} \quad \sin^2\theta + \rho^5_{00}\cos^2\theta \\
&\quad + \sqrt{2}\ \text{Re}\ \rho^5_{10}\sin 2\theta\cos\phi - \rho^5_{1-1} \quad \sin^2\theta\cos 2\phi\} \\
&- \sqrt{2\epsilon R(1+\epsilon+2\delta)}\sin\Phi\{\sqrt{2}\ \text{Im} \quad \rho^6_{10}\sin 2\theta\sin\phi + \text{Im}\ \rho^6_{1-1} \quad \sin^2\theta\sin 2\phi\}]. \qquad (9)
\end{aligned}
$$

(The negative sign in the last term differs from Reference [21]. We believe the negative sign is correct). R is the ratio of longitudinal to transverse cross section; $\delta = m_e/E \approx 0$. The transition amplitudes for the helicity conserving diffractive and pseudoscalar exchange scattering are incoherent; the two processes have additive terms in W [24].

The decay angles are defined relative to an appropriate coordinate system chosen to simplify $\rho^\alpha_{\lambda,\lambda'}$. For diffractive helicity conserving $\phi$ production choosing the helicity system, (z axis antiparallel to the outgoing proton direction making it to be parallel the $\phi$ momentum direction) yields:

$$B2) \qquad \rho^{\alpha}_{\lambda,\lambda'} = \rho^0, \rho^1, \rho^2, \rho^4, \rho^5, \rho^6 \qquad Diffraction$$

where $\rho^{\alpha}$ is defined in Appendix E of Reference [21].

$\rho^{\alpha}_{\lambda,\lambda'}$ for pseudoscalar exchange is obtained from the invariant amplitude for the upper ($\gamma_V$, PS, $\phi$) pseudoscalar exchange vertex. The amplitude is the contraction of the antisymmetric 4 tensor with the incoming $\gamma_V$ and outgoing $\phi$ 4-momenta and 4-spin functions [24]. Using the Gottfried Jackson frame (see Figure 20), in which the coordinate system z axis is parallel to $\gamma_v$, the invariant amplitude expression is greatly simplified: only transverse $\phi$ helicity obtain and the $\phi$ density matrices

$$B3) \qquad \rho^{\alpha}_{\lambda,\lambda'} = \rho^0, -\rho^1, -\rho^2 \qquad PS \;\; Xch$$

Expressions for pseudoscalar and diffractive W in the appropriate z axis systems are given in 1) and 2) respectively of this proposal. In 1) and 2), $\psi = \phi - \Phi$.

Following Reference [21], the helicity system was chosen for the purpose of this proposal. The pseudoscalar exchange, $\rho^{\alpha}_{\lambda,\lambda'}$, had to be rotated by angle $\alpha_{H \to GJ}$ from the Gottfried-Jackson frame into the helicity system.

$$B4) \qquad \alpha_{H \to GJ} = cos^{-1} \frac{\beta^* - cos\theta^*}{\beta^* cos\theta^* - 1}$$

where $\theta^*$ is the hadron cms scattering angle and $\beta^*$ is the velocity of the $\phi$ in the hadronic cms. $\alpha_{H \to GJ}$ increases rapidly from 0 at $t = t_{min}$. The increase of $\alpha_{H \to GJ}$ with t results in the $\phi$ unpolarized transverse (longitudinal) pseudoscalar exchange component decreasing (increasing) as t increases, providing a t signature for pseudoscalar exchange. At $t = t_{min}$, the unpolarized transverse component of the virtual photon gives only unpolarized transverse pseudoscalar exchange $\phi$s. This cannot be distinguished in W from the diffractive unpolarized transverse $\phi$s. As a result, at $t = t_{min}$, pseudoscalar exchange is distinguished from diffraction only in the two transverse - transverse components; the signs of PS $\rho^1$ and $\rho^2$ are opposite to those of diffraction, see B2) and B3) above.

In general, the unpolarized transverse and transverse-transverse pseudoscalar components rotated from the Gottfried Jackson frame into the helicity frame produce eight non-zero terms, with $\alpha = 0, 1, 2$, all proportional

to the amount of pseudoscalar scattering. Helicity conserving diffractive scattering has, in the same system, has 6 terms which can be grouped into 3 components, transverse unpolarized and transverse - transverse, (T, TT) with $\alpha = 1, 2$; longitudinal, (L), with $\alpha = 4$; transverse-longitudinal, (LT), with $\alpha = 5, 6$.

Hence pseudoscalar exchange and helicity conserving diffractive scattering will produce 4 components in W, 3 diffractive and one pseudoscalar exchange:

$$B5) \qquad W = f_{PS}W_{PS} + f_D^{T,TT}W_D^{TT} + f_D^L W_D^L + f_D^{LT}W_D^{LT}$$

where the angular arguments of W have been omitted for brevity. Using equations 105) and 106) of Reference [21],

$$B6) \qquad f_D^L \sim R \text{ and } f_D^{LT} \sim \sqrt{R}cos\delta$$

$\delta$ here is the phase angle of the longitudinal amplitude relative to the transverse in diffractive helicity conserving scattering. Using 3) and B6), the diffractive terms of B5) can be collected together and written as a function of $cos\delta$ and $\xi^2$, in addition to the decay angles. The final expression is given in 6).

# C Vector-Dominance Model

Diffractive production of vector mesons is normally analyzed within the context of the Vector-Meson Dominance (VMD) model. In this model it is assumed that in the interaction of photons with hadrons, the photon may be decomposed into a superposition of vector meson states, which subsequently scatter off the hadron [1]. Production of $\phi$'s though this mechanism may be interpreted in terms of the strange quark content of the photon. The diffractive cross section in the VMD model may be written as [4]

$$\frac{d^2\sigma}{dQ^2 dW dt} = (2\pi)\,\Gamma_W(Q^2,W)\,\zeta\,\sigma_t\,(1+\epsilon R)\,W_D(\cos\theta,\psi) \quad (10)$$

$$\sigma_t = \frac{A_\phi}{b_\phi}\exp(-b_\phi t') \quad (11)$$

$$t' = |t| - |t_-(Q^2)| \quad (12)$$

$$\zeta = \frac{W^2 - M_p^2}{2\,M_p^2\sqrt{\nu^2+Q^2}}\frac{1}{(1+\frac{Q^2}{M_\phi^2})^2} \quad (13)$$

$$\Gamma_W(Q^2,W) = \frac{\alpha}{8\pi^2}\frac{W}{M_p E_b^{\,2}}\frac{W^2 - M_p^2}{M_p Q^2}\frac{1}{1-\epsilon} \quad (14)$$

We use common designations for all variables: $Q^2$ and $\nu$ are the (negative) four-momenta and energy of the virtual photon; t is the four-momentum transfer from the proton to the vector meson (negative in this case); $\epsilon$ is the polarization of the virtual photon; $E_b$ is the energy of the electron beam; W is the mass of the hadronic system. $\Gamma_W(Q^2,W)$ is the flux of virtual photons. The normalization $\sigma_t$, in this model, is the cross section for real photons.[5] The factor $\zeta$ is used to extrapolate the cross section away from $Q^2 = 0$ and includes a propagator and a correction to the photon flux. The parameters which define the cross sections are taken from [33] and are shown in Table 4.

[4] See for example Reference [1] p. 375.

[5] Measurements with virtual photons find $\sigma_0$ to fall below the measured value with real photons [2].

# References


[1] T.H. Bauer *et al.*, Rev. Mod. Phys. **50**, 261 (1978).

[2] D.G. Cassel *et al.*, Phys. Rev. D **24**, 2787 (1981).

[3] EM Collab., J.J. Aubert *et al.*, Phys. Lett. **B161**, 203 (1985).

[4] M. Atkinson *et al.*, Z. Phys. C **30**, 521 (1986).

[5] L. Ahrens, *et al.*, Phys. Rev. D **35**, 785 (1987).

[6] T.P. Cheng and R.F. Dashen, Phys. Rev. Lett. **26**, 594 (1971); Phys. Rev. D. **13** 216 (1076).

[7] C.A. Dominguez and P. Langacker, Phys. Rev. D **24**, 1905 (1981).

[8] J. Gasser, H. Leutwyler and M.E. Sainio, Phys. Lett. **B253**, 252 (1991).

[9] D.B. Kaplan *et al.*, Nucl. Phys. **B310**, 527 (1988).

[10] M.D. Scadron, Z. Phys. C **54**, 595 (1992).

[11] J. Ellis *et al.*, Phys. Lett. **B217**, 173 (1989).

[12] R.L. Jaffee, Phys. Lett. **B229**, 275 (1989).

[13] "Measurement of the Flavor Singlet Charge Form Factor of the Proton, $G_E^0$," CEBAF Proposal PR-91-017, D.H. Beck, contact person.

[14] "Measurement of Strange Quark Effects Using Parity-Violating Elastic Scattering from $^4$He at $Q^2$=0.6," CEBAF Proposal PR-91-004, E. Beise, contact person.

[15] "Parity Violation in Elastic Scattering from the proton and $^4$He," CEBAF Proposal PR-91-010, P. Souder, contact person.

[16] E.M. Henley *et al.*, Phys. Lett. **B269**, 31 (1991).

[17] E.M. Henley *et al.*, Phys. Lett. **B281**, 178 (1991).

[18] E.M. Henley *et al.*, "Some Measurements for Determining Strangeness Matrix Elements in the Nucleon," XIIIth European Conference on Few-Body Problems in Physics, Marciana Marina, Island of Elba, Italy, 1991.

[19] J.J. Sakurai, Phys. Rev. Lett. **22**, 981 (1969).

[20] C.T. Day *et al.*, Phys. Rev. D **23**, 576 (1981).

[21] K. Schilling and G. Wolf, Nucl. Phys. **B61**, 381 (1973).

[22] K. Schilling *et al.*, Nucl. Phys. **B15**, 397 (1970).

[23] O. Dumbrajs *et al.*, Nucl. Phys. **B216**, 277 (1983).

[24] H. Fraas, Nucl. Phys. **B36**, 191 (1972).

[25] R.H. Dalitz, "The Production and Decay of Resonant States," in "Strong Interactions," Proceedings of the International School of Physics Enrico Fermi, 1966.

[26] H.J. Besh *et al.*, Nucl. Phys. **B70**, 257 (1974).

[27] LAMP2 Group, D.P. Barber *et al.*, Phys. Lett. **79B**, 150 (1978).

[28] H.-J. Behrend *et al.*, Nucl. Phys. **B144**, 22 (1978).

[29] D.W.G.S. Leigh, "High-Energy Photoproduction: Diffractive Processes," Electromagnetic Interactions of Hadrons, Vol. 1, Plenum Press, New York and London, A. Donnachie and G. Shaw, eds.

[30] A.H. Rosenfeld and P. Söding, "Photoproduction of Vector Mesons – Experimental," International School of Subnuclear Physics, Erice, Italy, 1971, A. Zichichi, ed.

[31] J. Ballam *et al.*, Phys. Rev. D **7**, 3150 (1973).

[32] H.J. Halpern *et al.*, Phys. Rev. Lett. **29**, 1425 (1972).

[33] R. Dixon *et al.*, Phys. Rev. Lett. **39**, 516 (1977).

[34] W.D. Shambroom *et al.*, Phys. Rev. D **26**, 1 (1982).

[35] E.S. Smith, "Fast Monte Carlo Program for the CLAS Detector," CLAS-NOTE-90-003, February, 1990.

[36] H. Fraas and D. Schildknecht, Nucl. Phys. **B14**, 543 (1969).

[37] "Review of Particle Properties," Particle Data Group, Phys. Lett. **B204**, 1988.

Table 1: We give the expected contamination (%) of the three $\Lambda^*$ resonances as a function of hadronic mass W. Also given is the efficiency loss for the $\phi$ sample if the the contamination of the $\Lambda^*$resonances is reduced to less than 3%.

| *W(GeV²)* | *Contamination* | Efficiency Loss |
|---|---|---|
| 2.1 | 6% | 2% |
| 2.2 | 10% | 15% |
| 2.3 | 5% | 12% |
| 2.4 | 3% | 2% |
| 2.5 | 0% | 0% |

# List of Figures

Table 2: Existing $\phi$ production data.

| Data | W (GeV) | t (GeV$^2$) | $\rho^{\alpha}_{\lambda,\lambda'}$ | $f_{PS}$ |
|---|---|---|---|---|
| Ref. [27] | 3. | 0.4 | $\rho^0_{00}$, $\rho^0_{1-1} = 0.0 \pm 0.2$ | $\leq 50\%$ |
| $\gamma$ | | | $\rho^0_{10} = 0.00 \pm 0.05$ | $\leq 30\%$ |
| Ref. [28] | 3. | 0.1 | $\rho^0_{00}$,$\rho^0_{1-1}$,$\rho^0_{10} = 0.00 \pm 0.10$ | $\leq 40\%$ |
| Ref. [32] | 5. | $0.02 \leq t \leq 0.8$ | $\rho^0_{00}$, $\rho^0_{1-1}$, $\rho^0_{10} = 0.00 \pm 0.08$ | $\leq 30\%$ |
| Polarized | | | $\rho^1_{00}$, $\rho^1_{11}$, $\rho^1_{10}$, $\rho^2_{10} = 0.00 \pm 0.10$ | $\leq 40\%$ |
| $\gamma$ | | | $\rho^1_{1-1} = 0.18 \pm 0.13$ | $\leq 30\%$ |
| | | | $\rho^2_{1-1} = 0.51 \pm 0.16$ | $\leq 30\%$ |
| Ref. [33] | 3 | $0. \leq t \leq 1.$ | from Fig. 4, $\psi$ distribution | $\leq 50\%$ |
| e e' | | | from Fig. 4, $\cos\theta$ distribution | $\leq 70\%$ |

Table 3: Detection mode efficiencies. These percentages are not exclusive. The analysis cuts to select the tracks include good tracking and particle identification and a $2.5\sigma$ cut on the K+K- missing mass.

| *Mode* | *Efficiency* |
|---|---|
| $e^-K^+K^-p$ | 1.1% |
| $e^-K^+K^-$ | 1.2% |
| $e^-pK^+$ | 7.8% |
| $e^-pK^-$ | 3.7% |
| $e^-$ and 2 of $pK^+K^-$ | 10.8% |

Table 4: The detector acceptance was computed with FASTMC and includes the detection of the electron, the proton and at least one kaon. Each entry corresponds to the events expected in a bin with $\Delta Q^2 = 0.2$ GeV$^2$/c$^2$ and $\Delta W = 0.1$ GeV. The acceptance is expressed as a percentage.

| | | $Q^2$ | | | | | | | | | |
|---|---|---|---|---|---|---|---|---|---|---|---|
| | | 0.1 | 0.3 | 0.5 | 0.7 | 0.9 | 1.1 | 1.3 | 1.5 | 1.7 | 1.9 |
| | 2.05 | 0 | 4.6 | 7.3 | 8.6 | 10.7 | 12.8 | 12.6 | 13.1 | 12.4 | 11.6 |
| | 2.15 | 0 | 7.3 | 9.9 | 11.3 | 13.1 | 14.1 | 14.9 | 14.2 | 13.2 | 13.1 |
| W | 2.25 | 0 | 0 | 12.1 | 14.6 | 14.9 | 14.7 | 14.9 | 15.1 | 14.6 | 14.2 |
| | 2.35 | 0 | 0 | 12.3 | 14.1 | 16.1 | 16.2 | 15.9 | 15.2 | 14.8 | 1.4 |
| | 2.45 | 0 | 0 | 0 | 14.7 | 14.9 | 15.8 | 12.6 | 1.6 | 1.1 | 0.6 |

Table 5: Expected rate of $\phi$ mesons produced with a 350-hour run with the CLAS detector at a luminosity of 10nb$^{-1}$s$^{-1}$. The rates are based on cross sections for diffractive production given in Appendix C, a 49% branching fraction into $K^+K^-$and missing mass cuts mentioned in the text.

| | | $Q^2$ | | | | | | | | | |
|---|---|---|---|---|---|---|---|---|---|---|---|
| | | 0.1 | 0.3 | 0.5 | 0.7 | 0.9 | 1.1 | 1.3 | 1.5 | 1.7 | 1.9 |
| | 2.05 | 0 | 1671 | 825 | 374 | 205 | 115 | 57 | 31 | 15 | 8 |
| | 2.15 | 0 | 3398 | 1544 | 727 | 392 | 213 | 119 | 62 | 33 | 19 |
| W | 2.25 | 0 | 0 | 2178 | 1145 | 571 | 293 | 164 | 95 | 54 | 32 |
| | 2.35 | 0 | 0 | 2393 | 1233 | 707 | 383 | 213 | 120 | 70 | 4 |
| | 2.45 | 0 | 0 | 0 | 1353 | 705 | 415 | 192 | 16 | 6 | 2 |

Table 6: Values of the parameters used to define the cross section for $\phi$ production in the VMD model. The quoted parameters are for the *average* values over $Q^2$ and W from references [33, 2].

| *Parameter* | *Value* |
|---|---|
| $\xi^2$ | $0.33 \pm 0.08$ |
| $\cos\delta$ | $0.7 \pm 0.7$ |
| $A_\phi$ | $1\ \mu b/GeV^2$ |
| $b_\phi$ | $3.46 \pm 0.22\ /GeV^2$ |

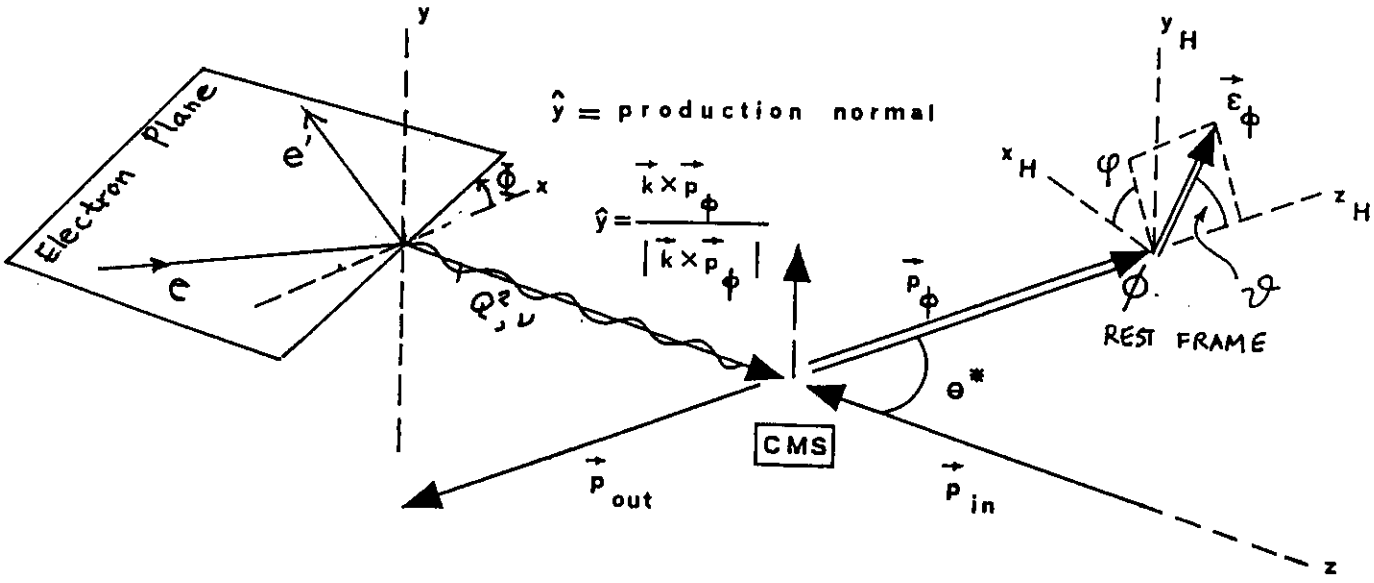


Figure 1: Sketch of the electroproduction of $\phi$ mesons. The virtual photon delivers $Q^2$ and energy transfer $\nu$. The electron scattering plane is at an angle $\Phi$ relative to the hadron production plane. The decay angles of the $K^+$ from the $\phi$ vector meson decay is also shown.

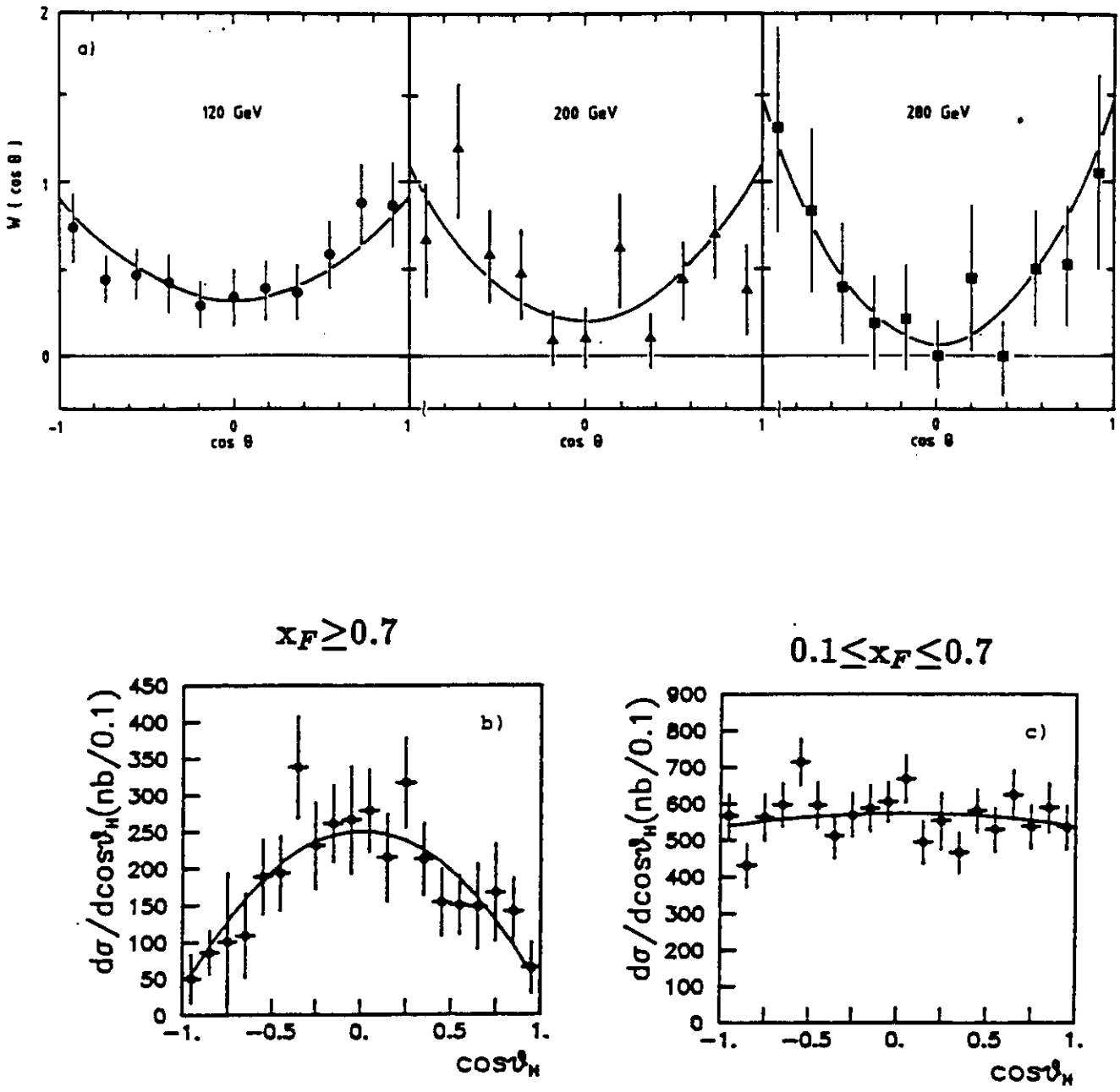


Figure 2: Decay distributions from vector meson decays at high energy. a) Decay distribution of $\rho \rightarrow \pi^+\pi^-$ in exclusive muoproduction [3] showing primarily a $\cos^2\theta$ distribution. b) Decay of $\phi \rightarrow K^+K^-$ in inclusive photoproduction (Reference [4]). The angular correlation shows different production mechanisms are responsible for $\phi$ production in different regions of $x_F$.

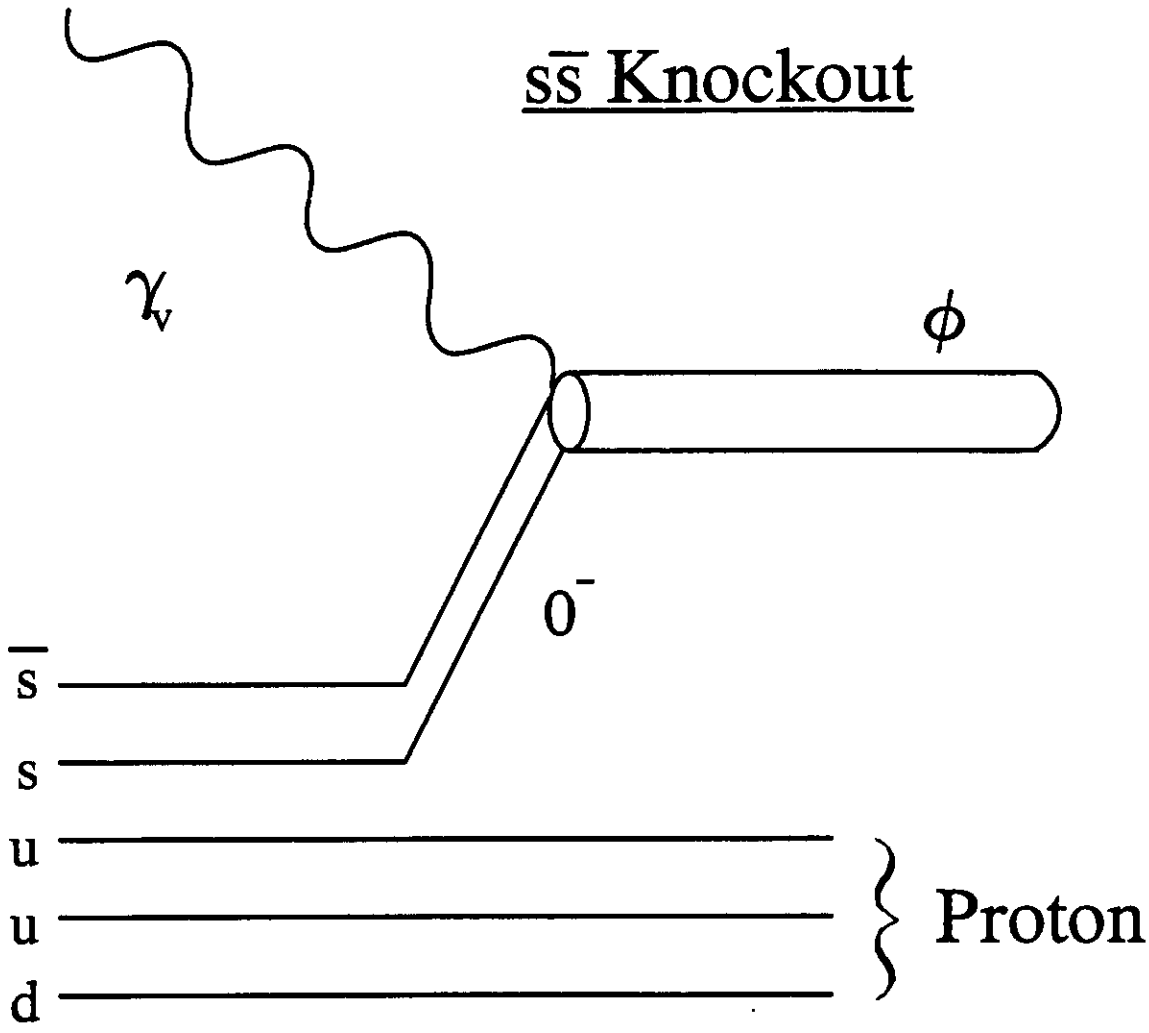


Figure 3: Schematic diagram of $\phi$ production by $s\bar{s}$ knockout as calculated in Reference [17].

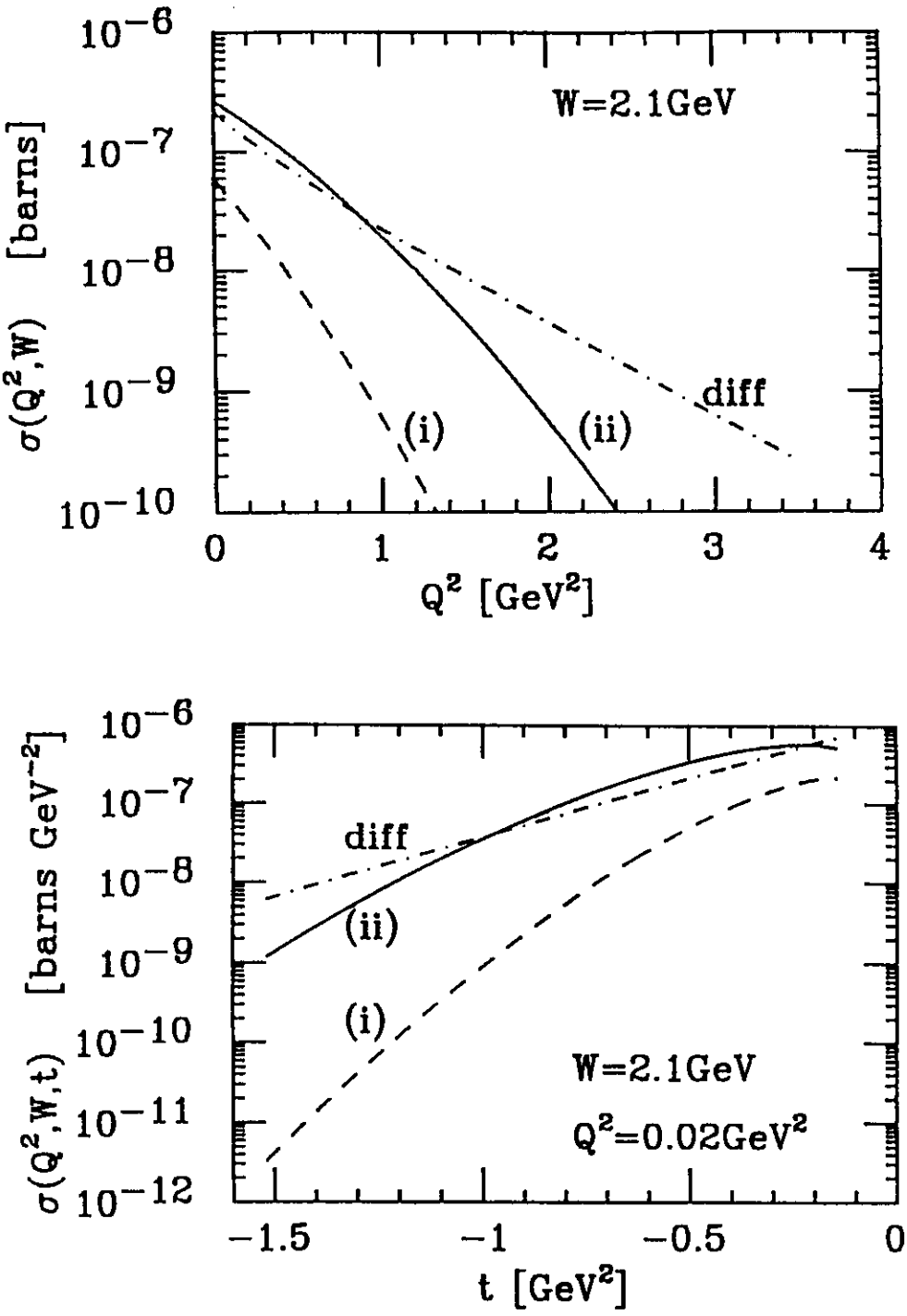


Figure 4: Cross section calculations of $\phi$ production by $s\bar{s}$ knockout from Reference [17].

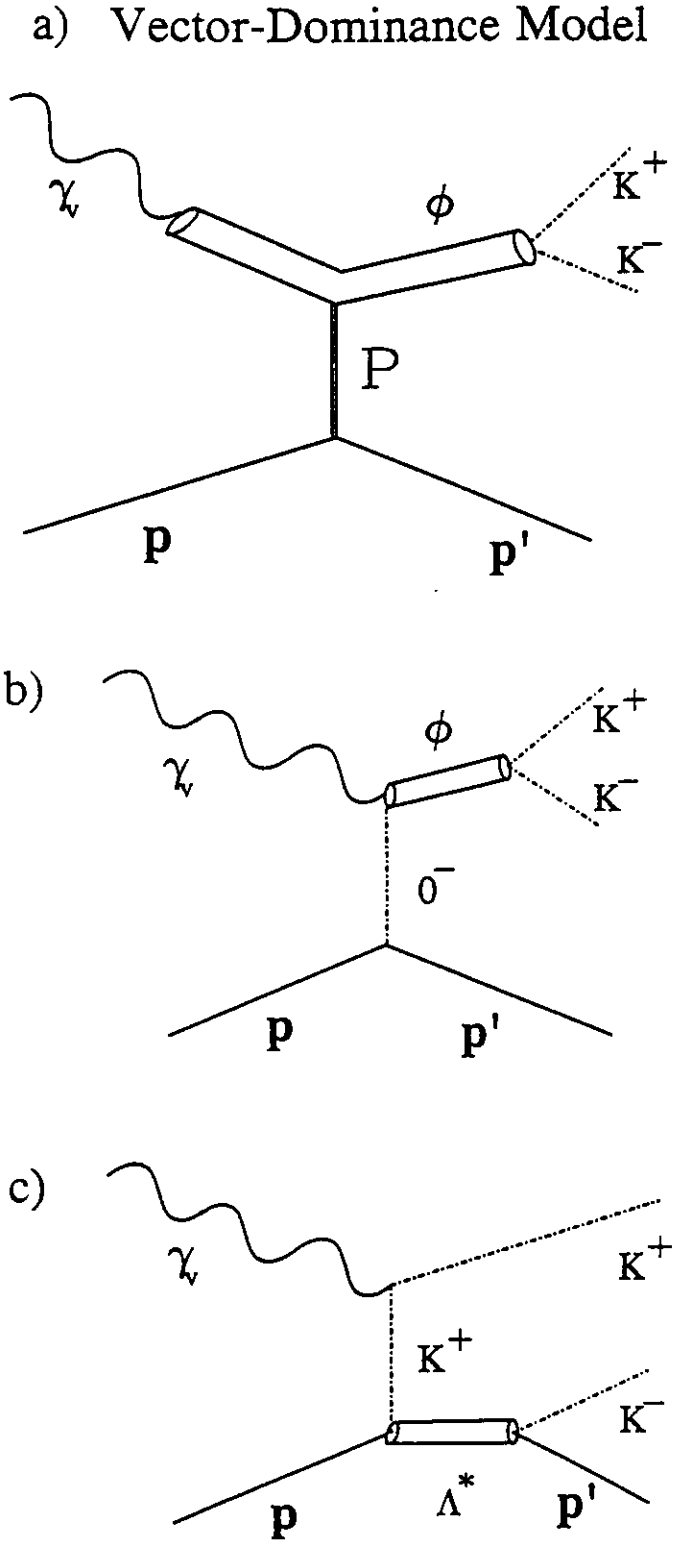


Figure 5: Three mechanisms for $K^+K^-$pairs are shown schematically a) diffraction, b) pseudoscalar meson exchange and c) production of high mass strange baryons.

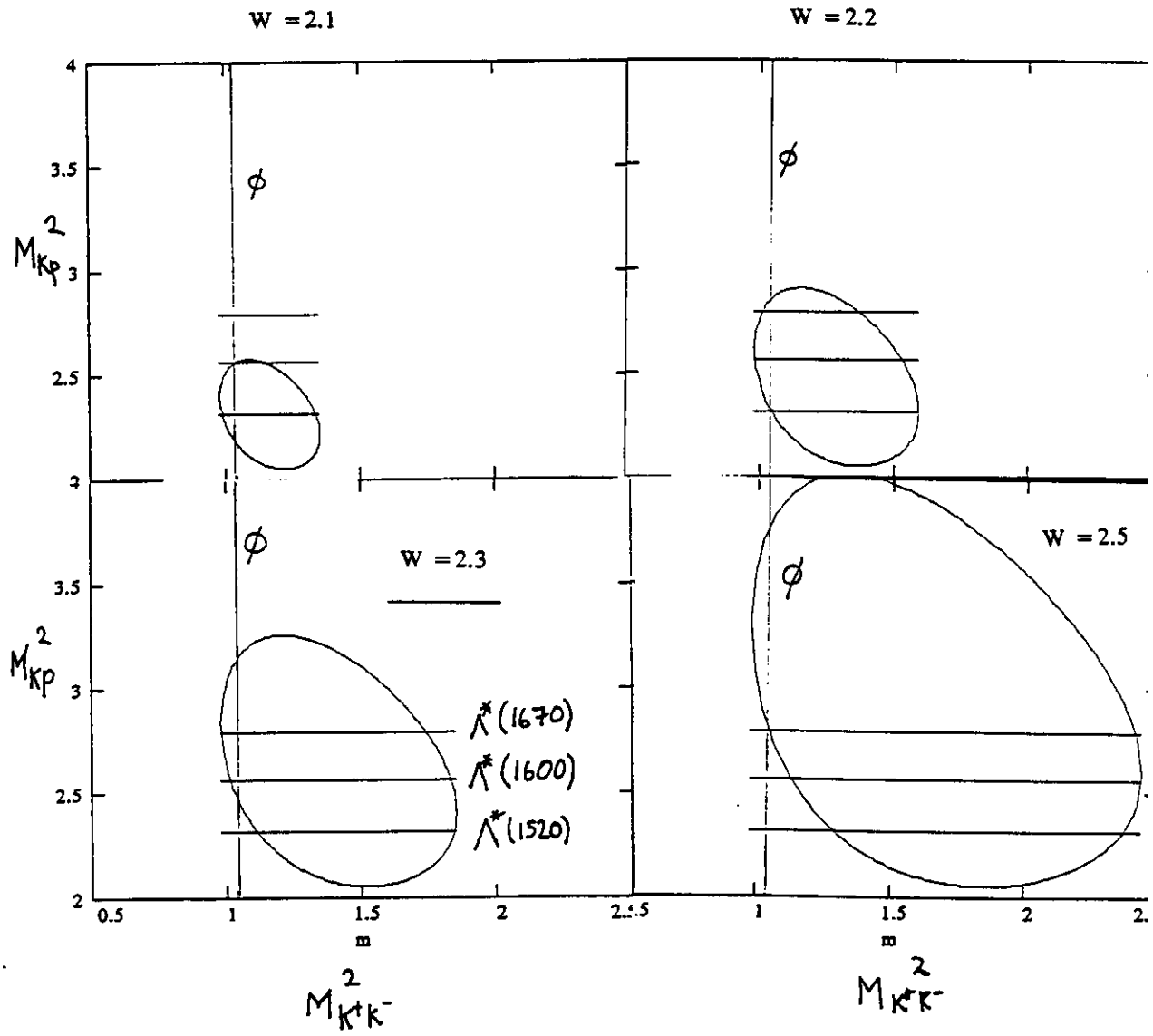


Figure 6: We give the Dalitz plots for the production of $K^+$, $K^-$ and p at fixed W. Note how the resonances $\Lambda^*(1520)$, $\Lambda^*(1600)$and $\Lambda^*(1670)$fall under different portions of the $\phi$ mass peak.

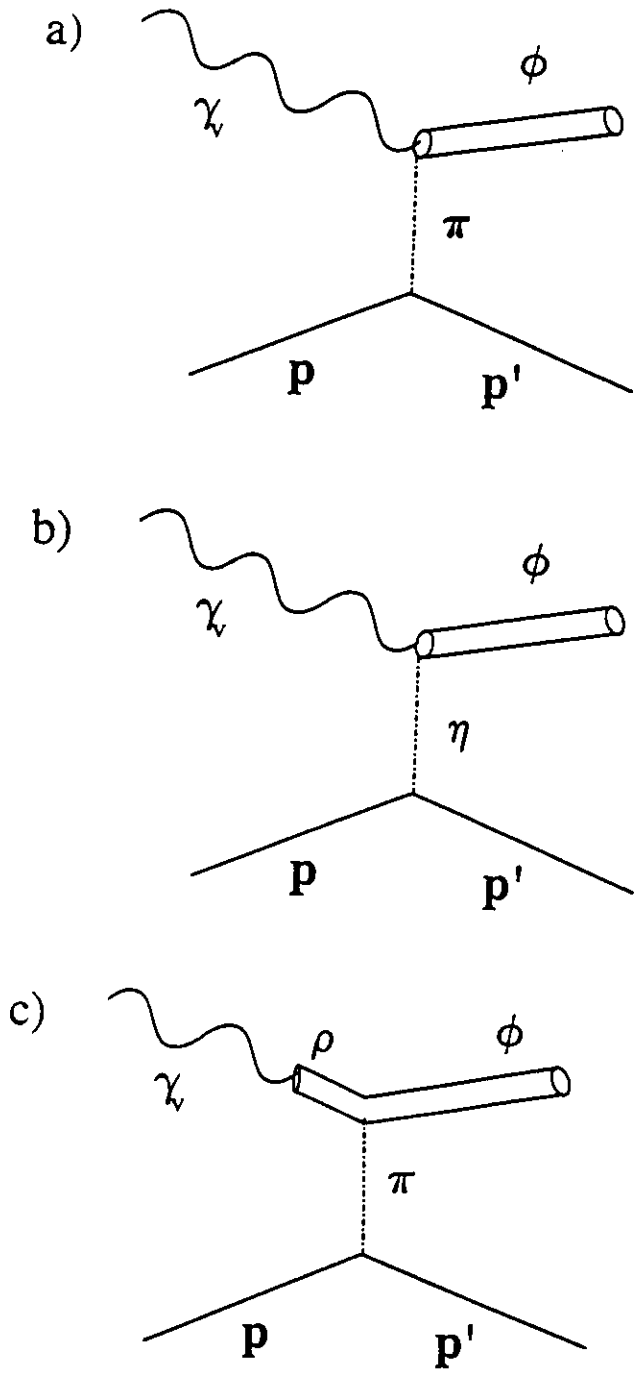


Figure 7: Diagrams for the exchange of $\pi$ and $\eta$ mesons in the t-channel.

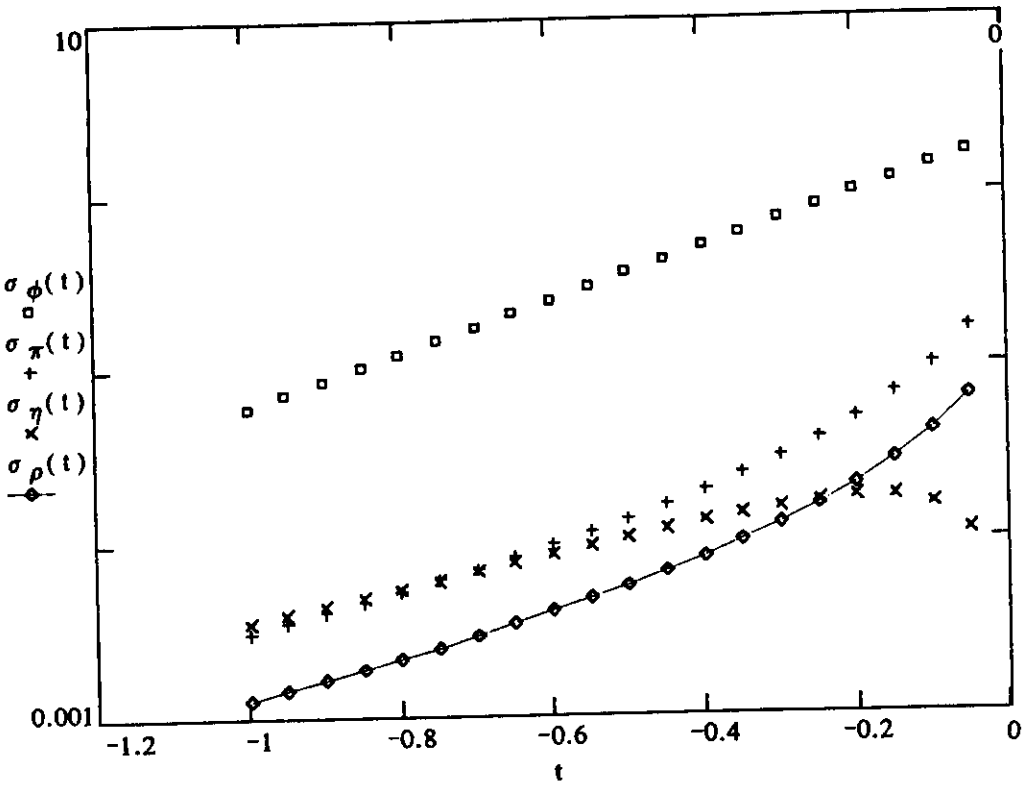


Figure 8: Rate estimates for the exchange of $\pi$ and $\eta$ mesons assuming incoherent addition. However, the diagrams are expected to interfere destructively, reducing the calculated values. The total rate of these diagrams relative to diffractive production is expected to be $\leq 5\%$.

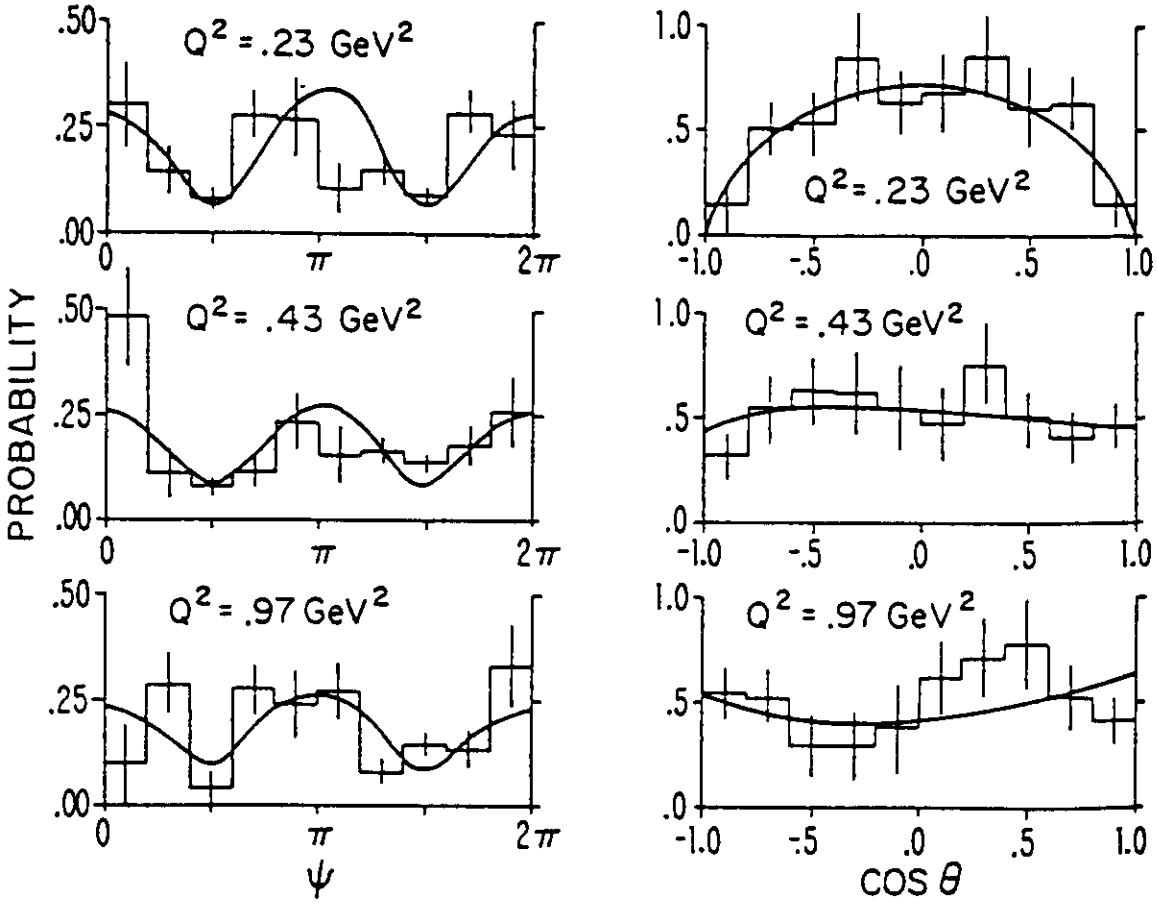


Figure 9: These are the only published angular distributions of the $K^+$ in the rest frame of the $\phi$ for the exclusive reaction $ep \rightarrow K^+K^-p$. They are taken from Reference [33].

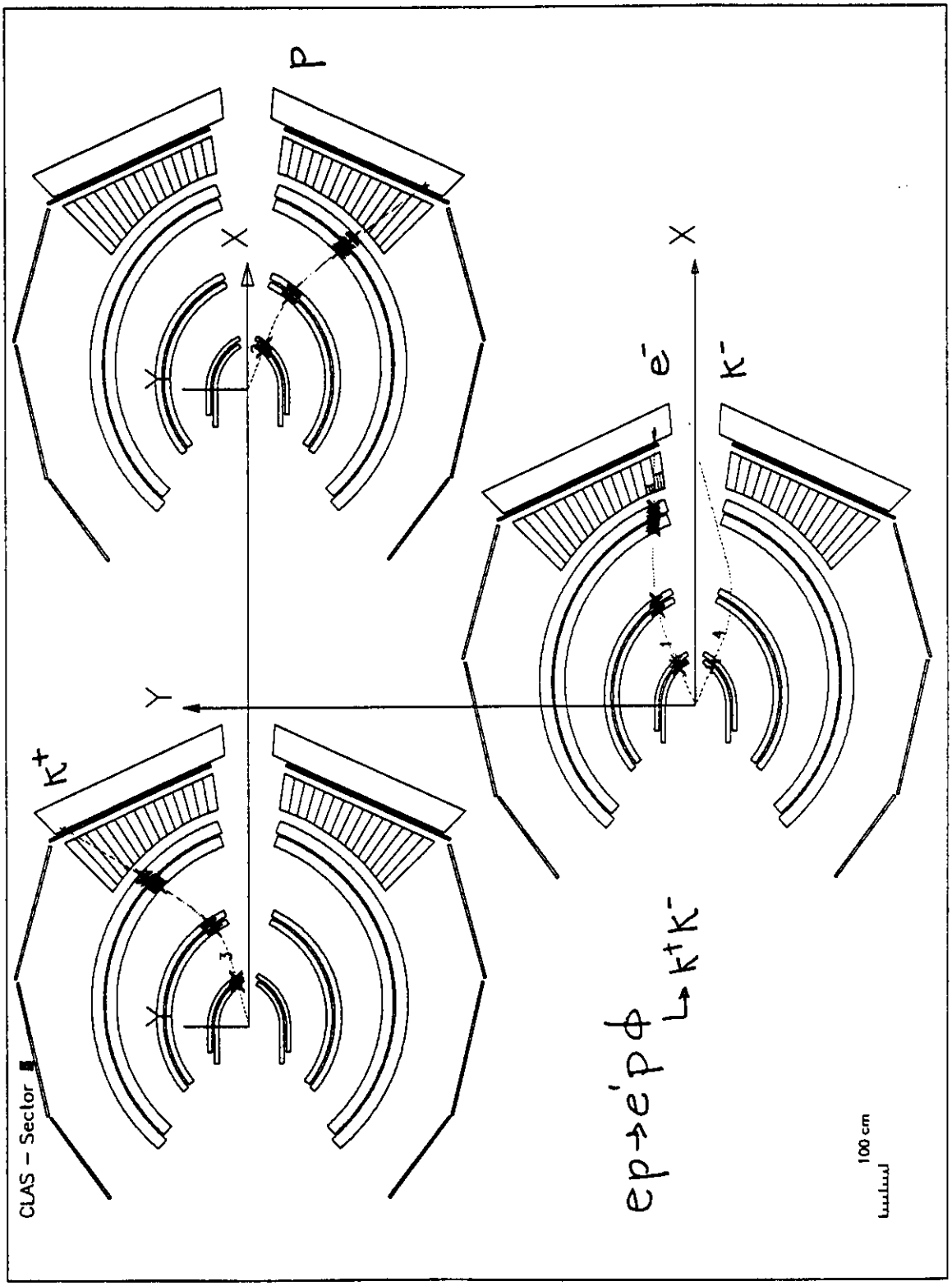


Figure 10: Single event display of the CLAS detector for ep→$K^+K^-$p. The $K^-$was not detected.

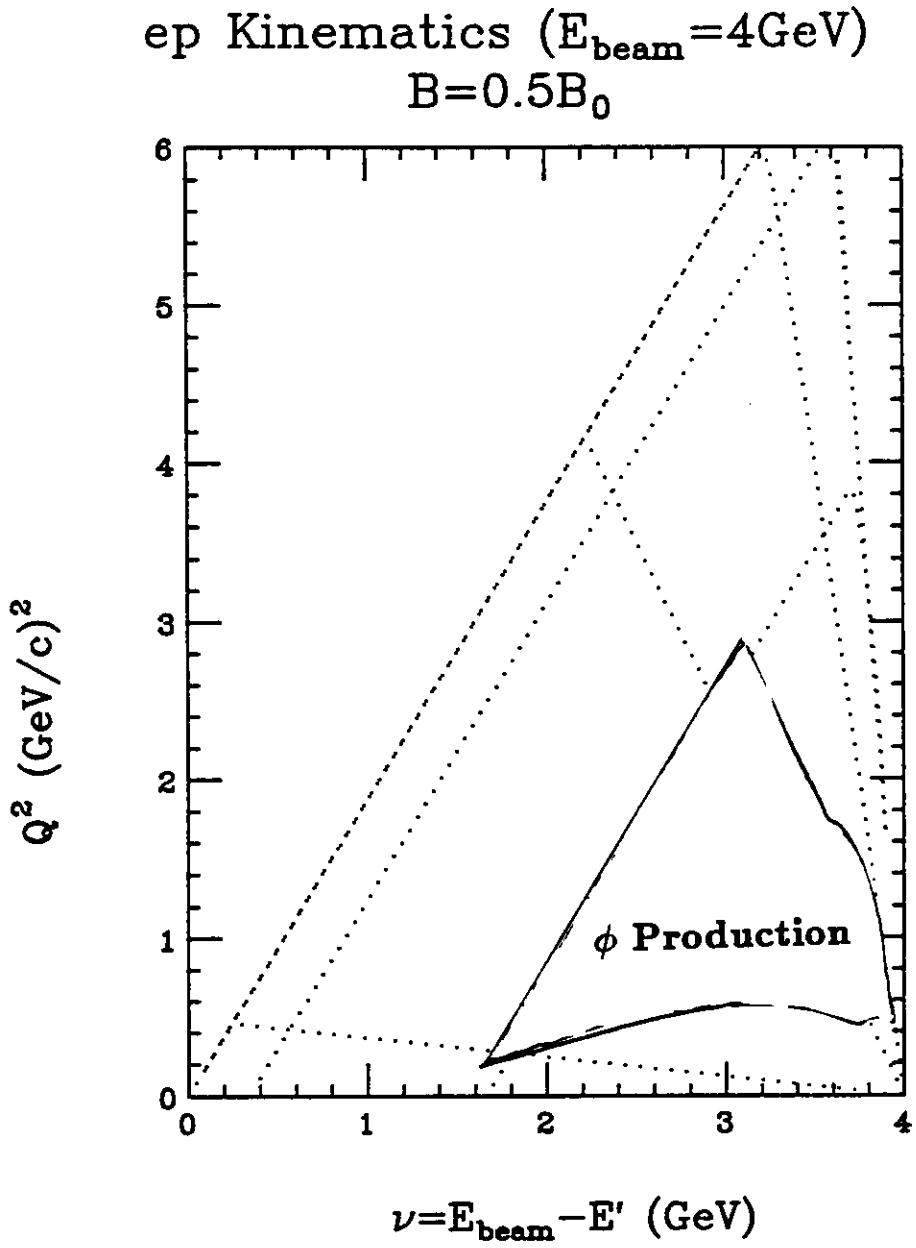


Figure 11: Acceptance region for the electron for $Q^2$ vs $\nu$ at 4 GeV. The magnetic field is set at half its nominal value and electrons are bent toward the beam axis.

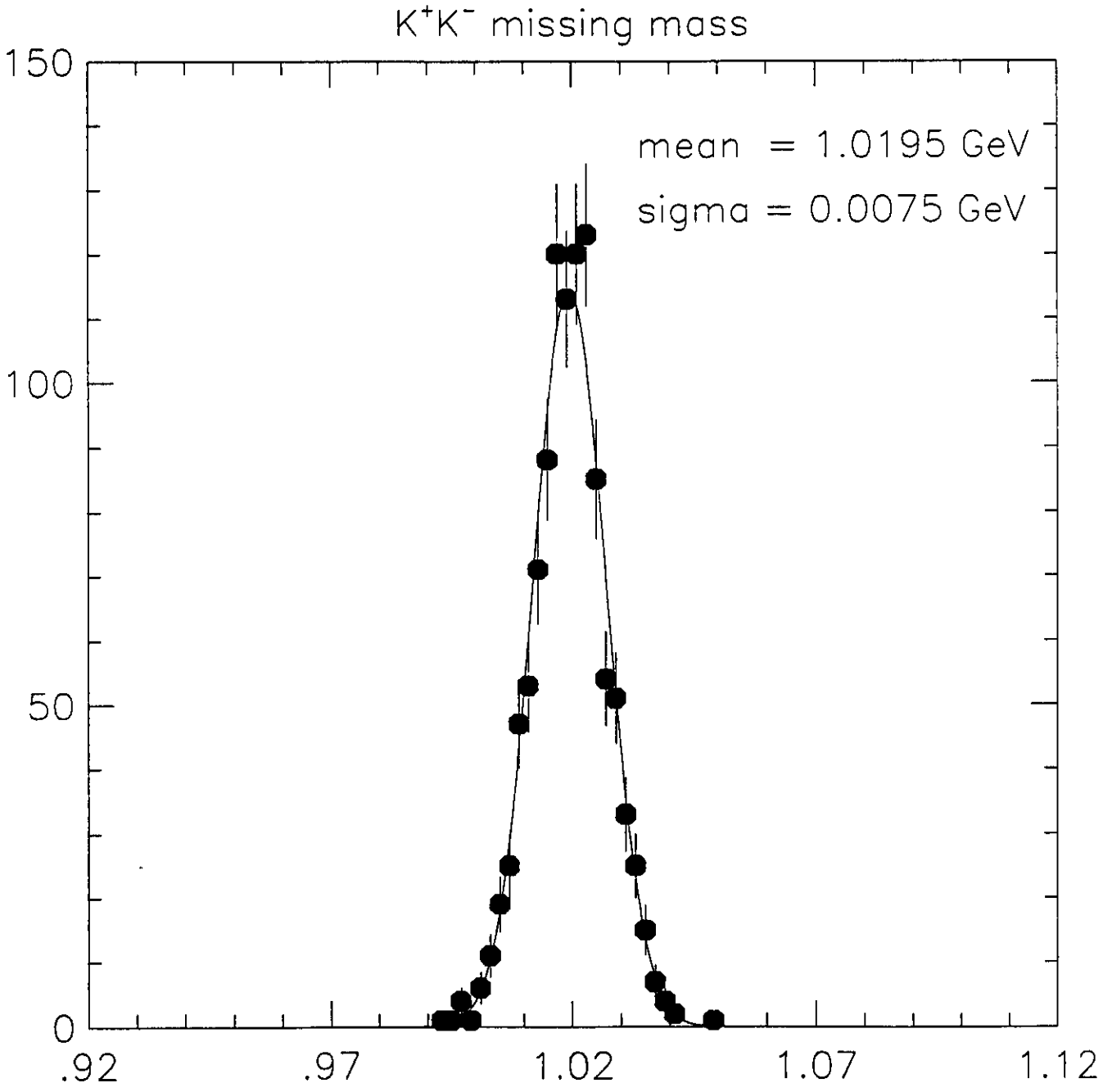


**Figure 12: The resolution of the $\phi$ mass has a width of 7.5 MeV, which allows rejection of backgrounds due to $K^+K^-$pairs not originating from $\phi$ decay.**

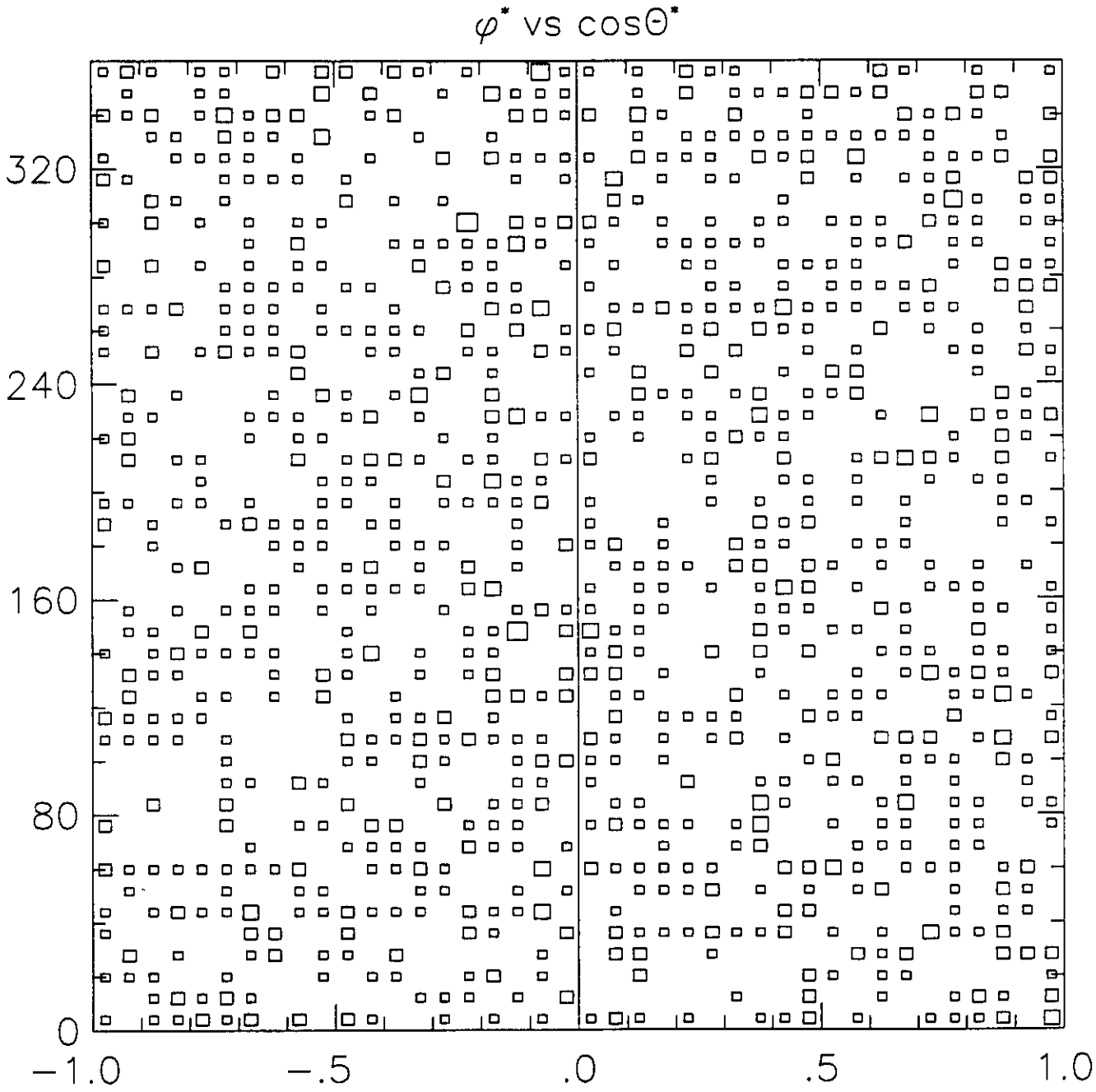


**Figure 13: The acceptance of the detector is uniform over the available phase space for decay of the $K^+$ in the rest frame of the $\phi$.**

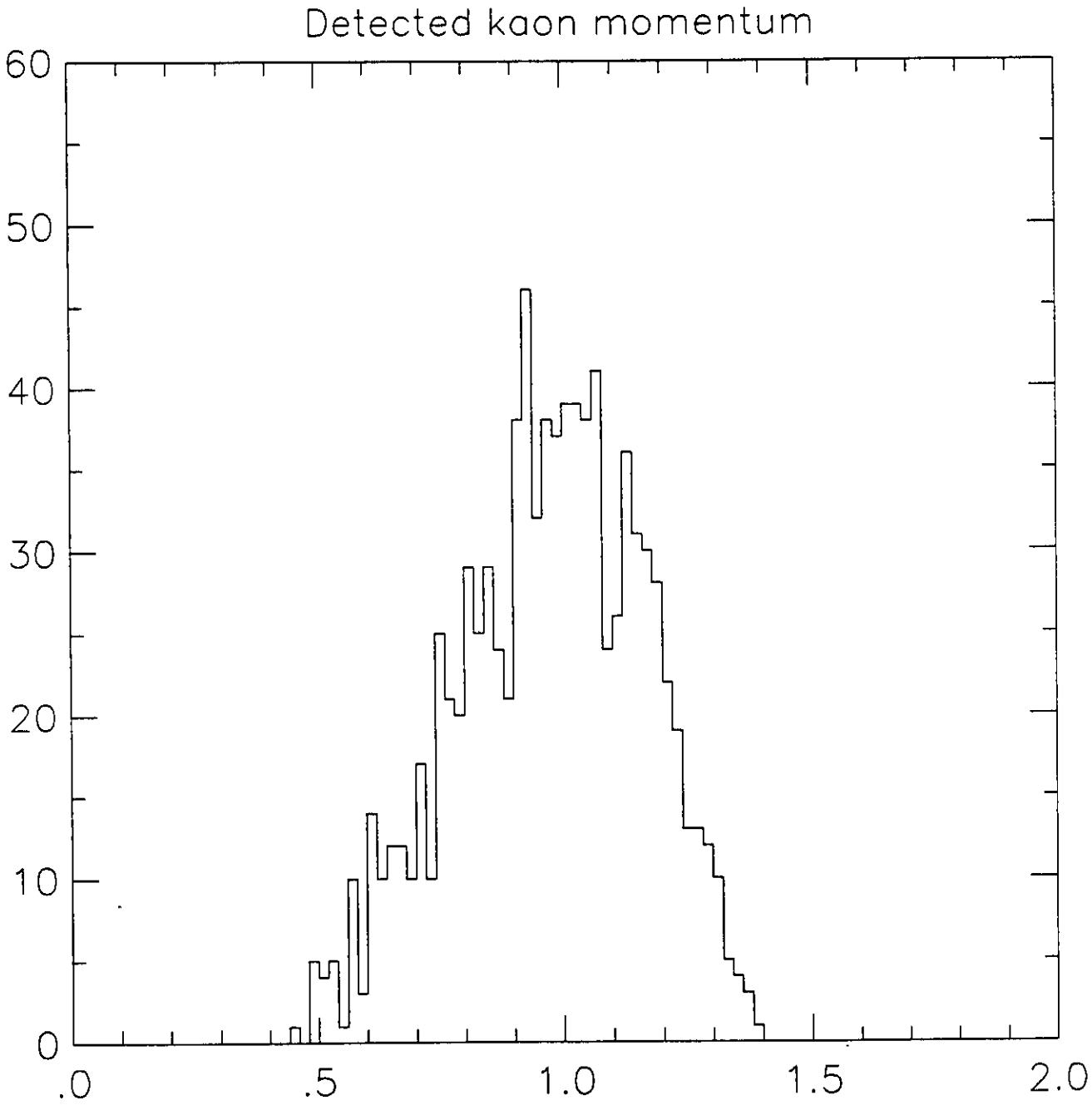


**Figure 14: Momentum spectrum of detected kaons. The particle identification by TOF of the CLAS detector can distinguish pions from kaons up to 2 GeV.**

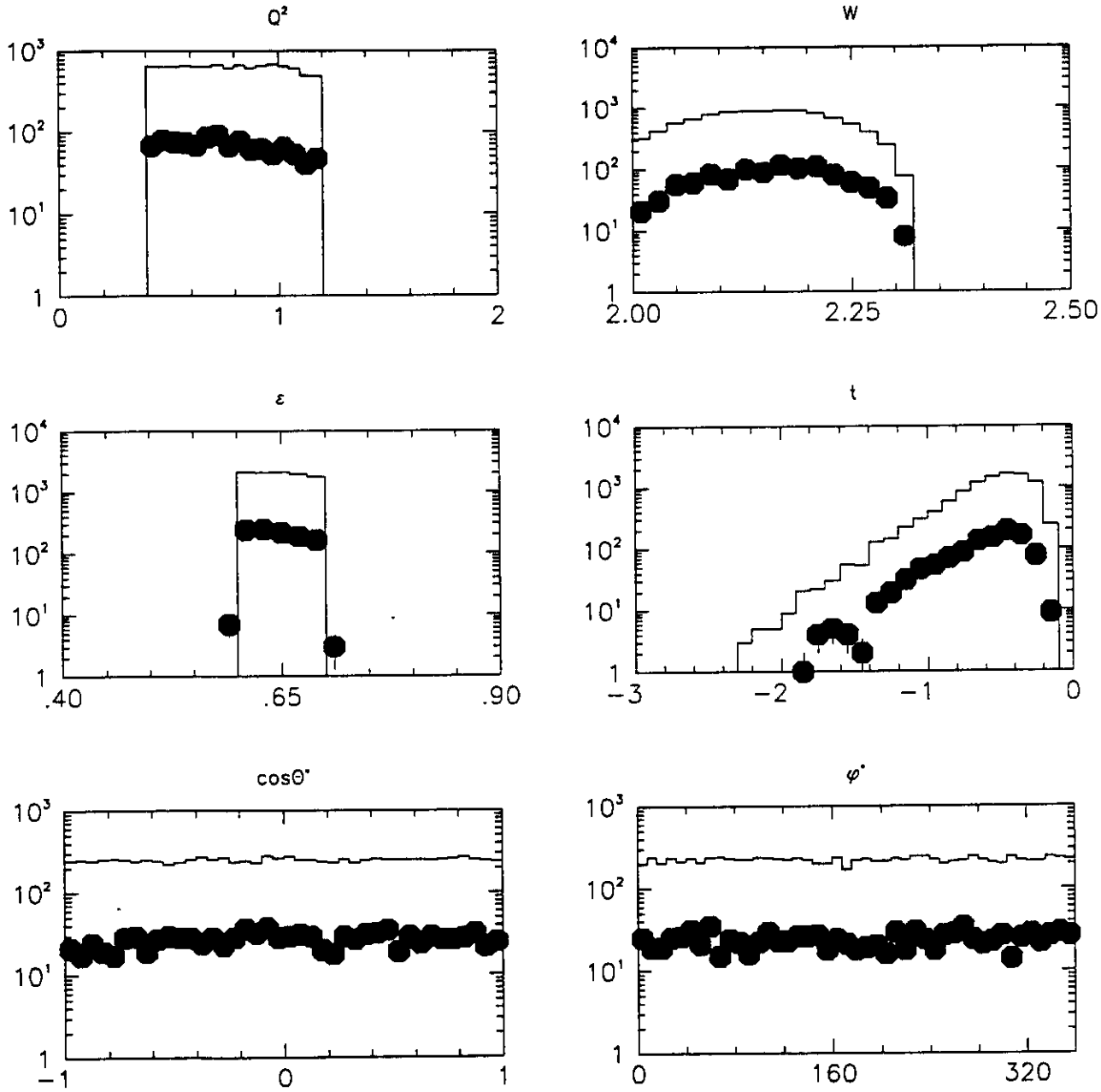


Figure 15: Acceptance of the reaction ep→$K^+K^-$p as a function of the kinematic variables $Q^2$, W, $\epsilon$, t, and the $K^+$ decay angles $\cos\theta$ and $\varphi$. In all cases the acceptance is quite uniform and ~10%.

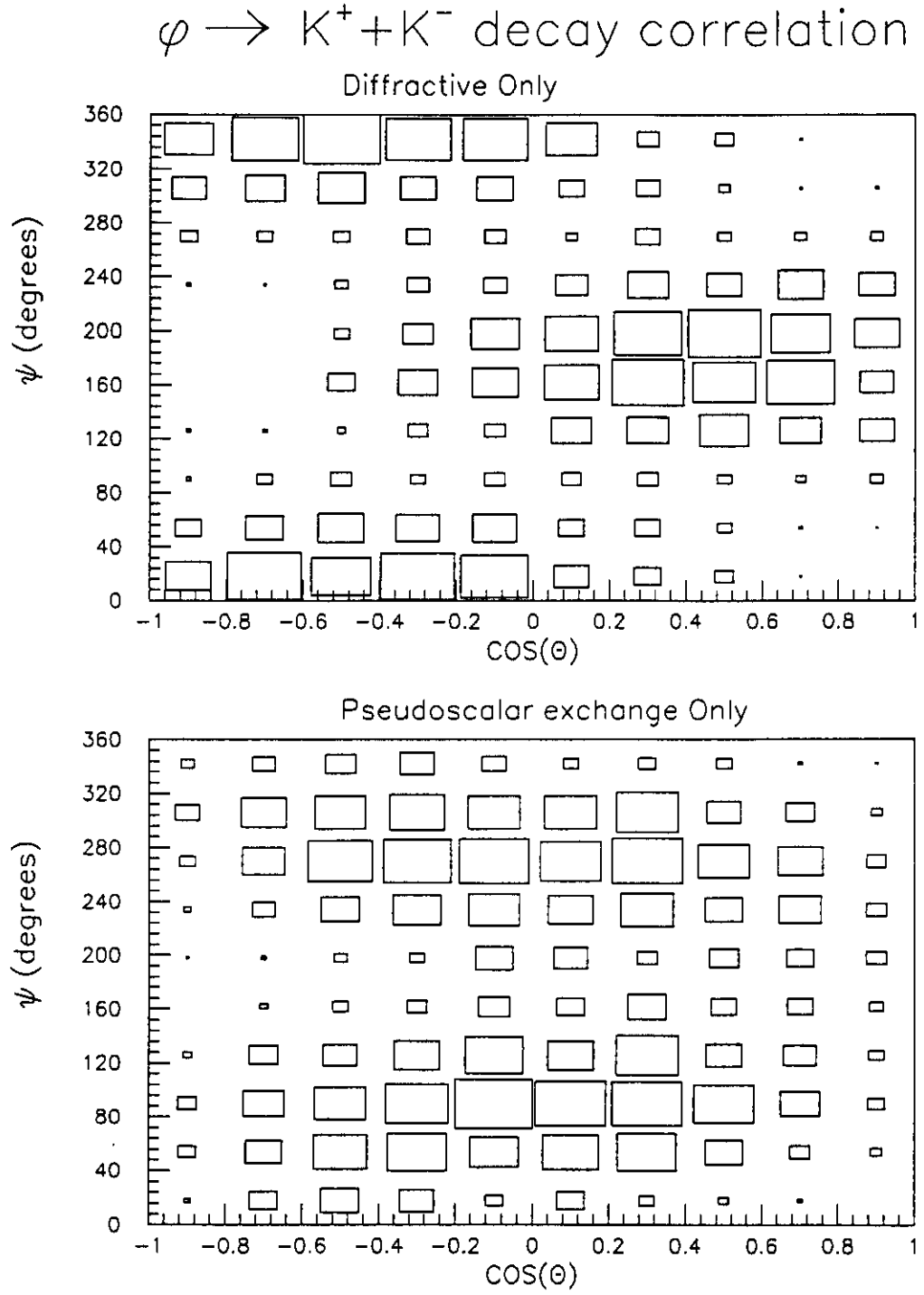


**Figure 16: Decay distribution as a function of $\cos\theta$ and $\psi$ for a) pure diffractive and b) pseudoscalar exchange. We note the substantial difference in these two-dimensional distributions is lost when one integrates over either $\cos\theta$ or $\psi$.**

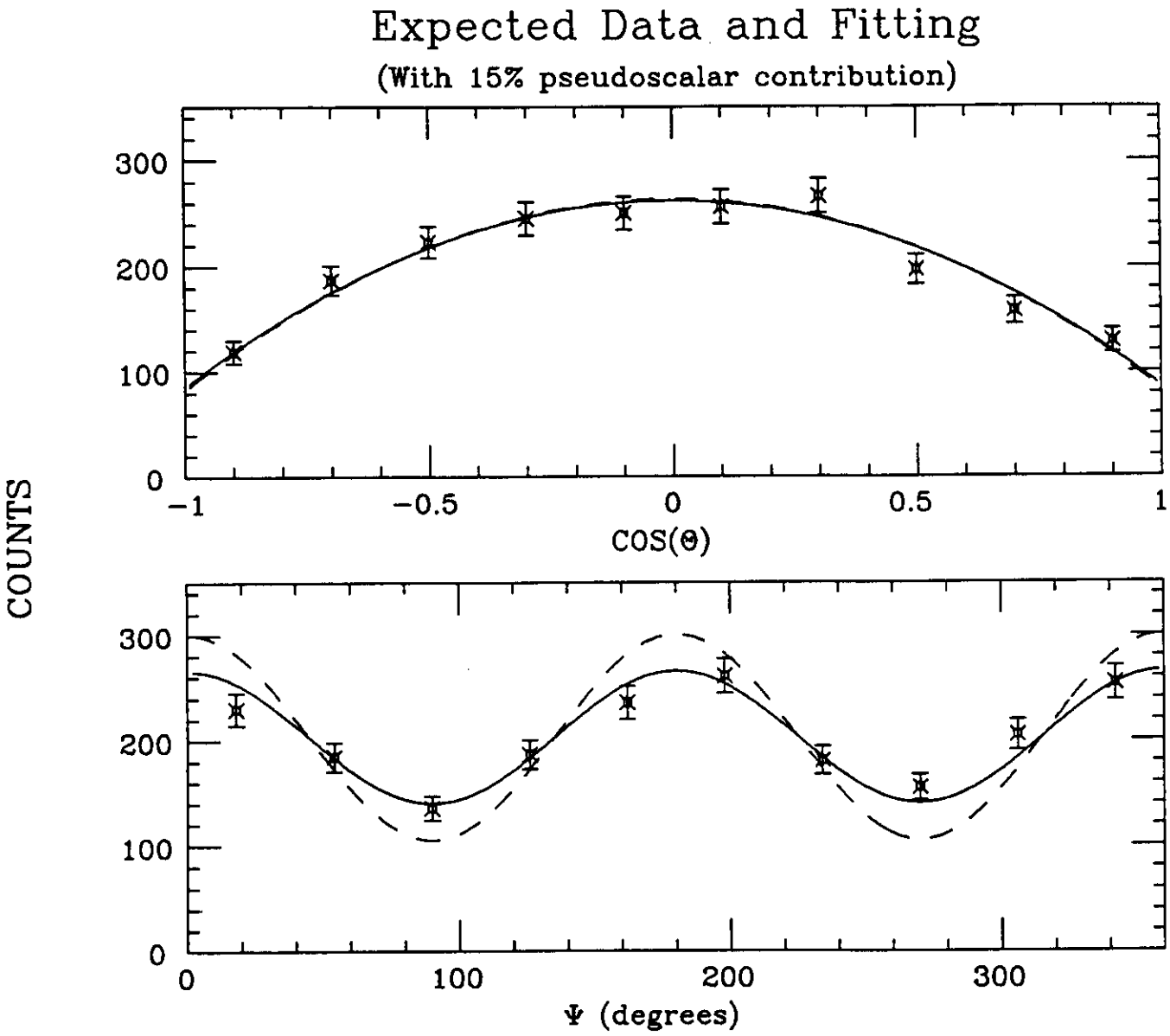


Figure 17: Fits to the $\phi$ decay distribution projected onto two one-dimensional plots. The input distributions were generated assuming 15% pseudoscalar exchange. The solid curve shows the fit including this component. The dashed curve shows the expected distribution for pure diffraction. In the projection, the $\cos\theta$ distribution appear insensitive to the pseudoscalar component.

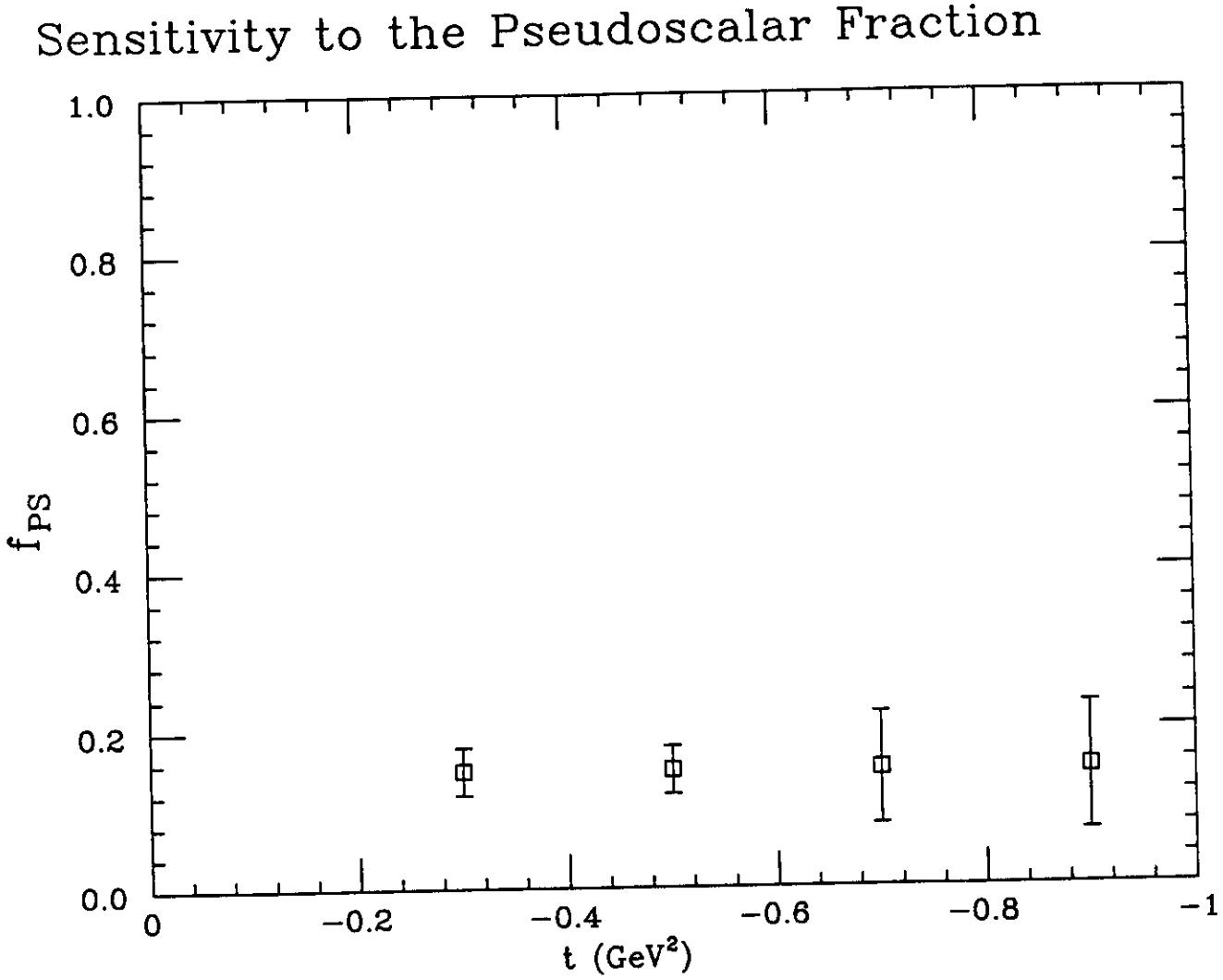


**Figure 18: Expected sensitivity to pseudoscalar exchange as a function of t. The errors include statistical uncertainties in the generated distribution, as well as systematic shifts in the fitting procedure. The fits allowed $f_{PS}$, $f_D$, R and $\cos\delta$ to be determined independently.**

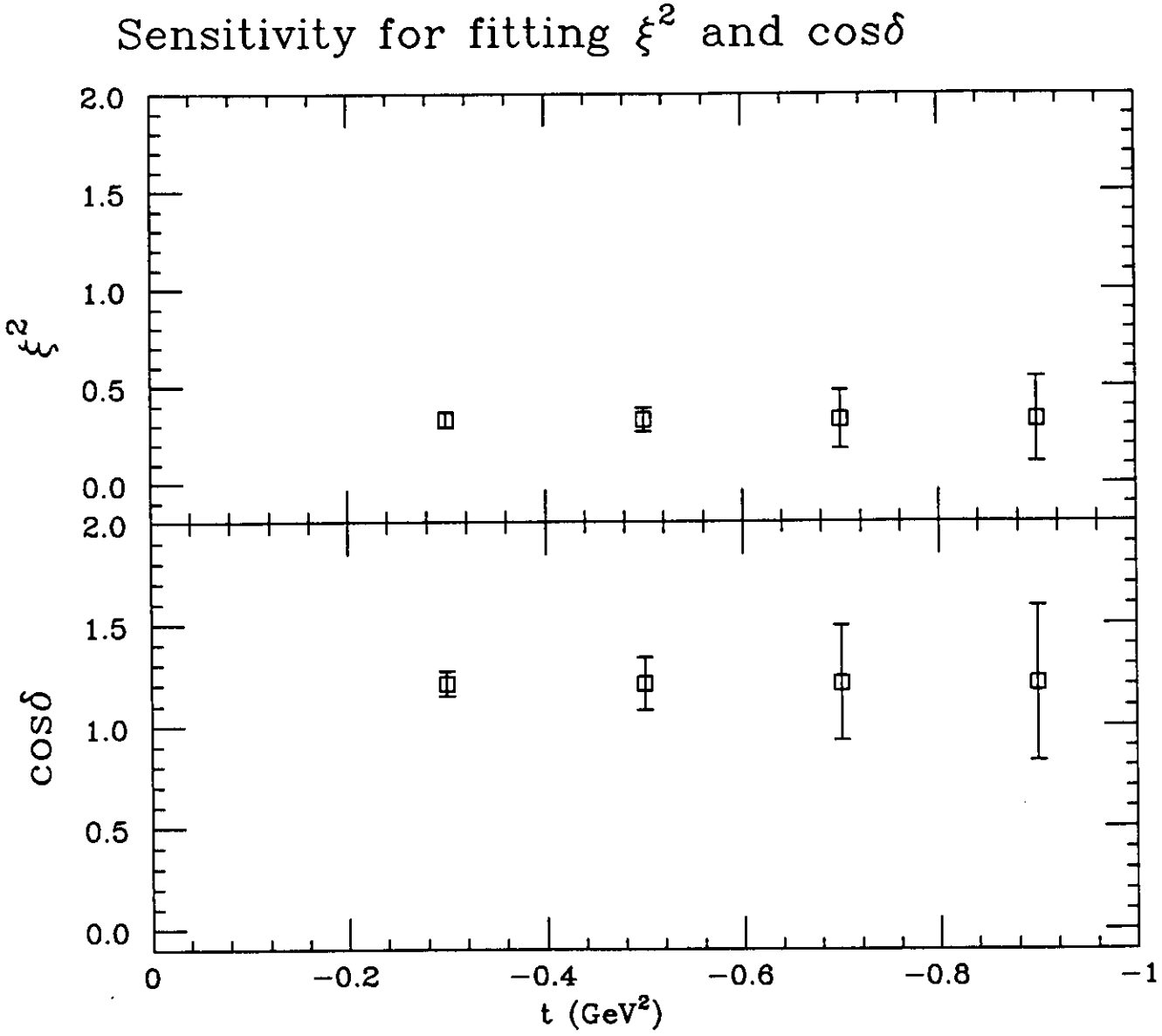


**Figure 19** Expected sensitivity to $\xi^2$ and cos$\delta$ as a function of t. The errors include statistical uncertainties in the generated distribution, as well as systematic shifts in the fitting procedure. The fits allowed $f_{PS}$, $f_D$, $\xi^2$ and cos$\delta$ to be determined independently.

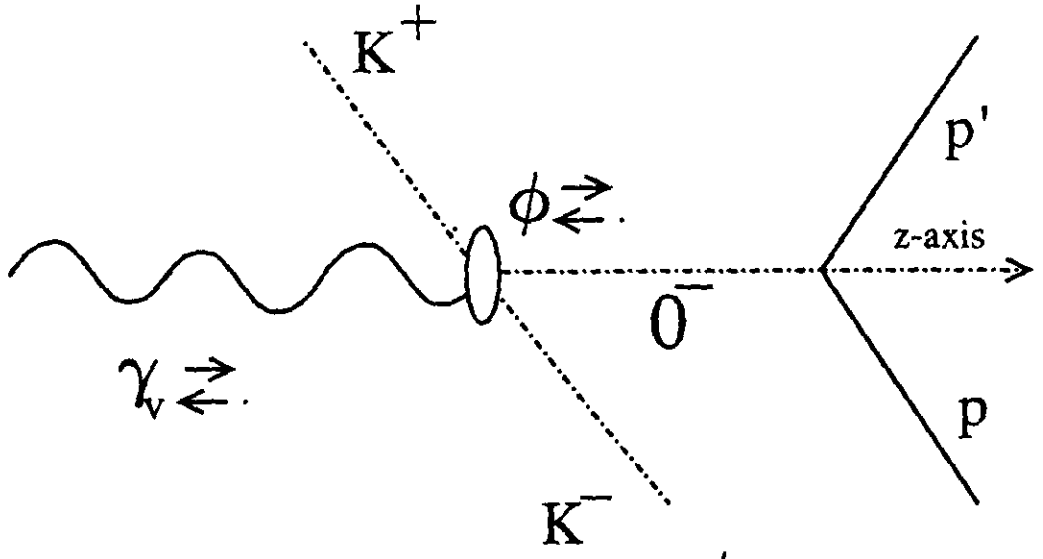


a) Gottfried-Jackson Frame ($\phi$ rest frame)

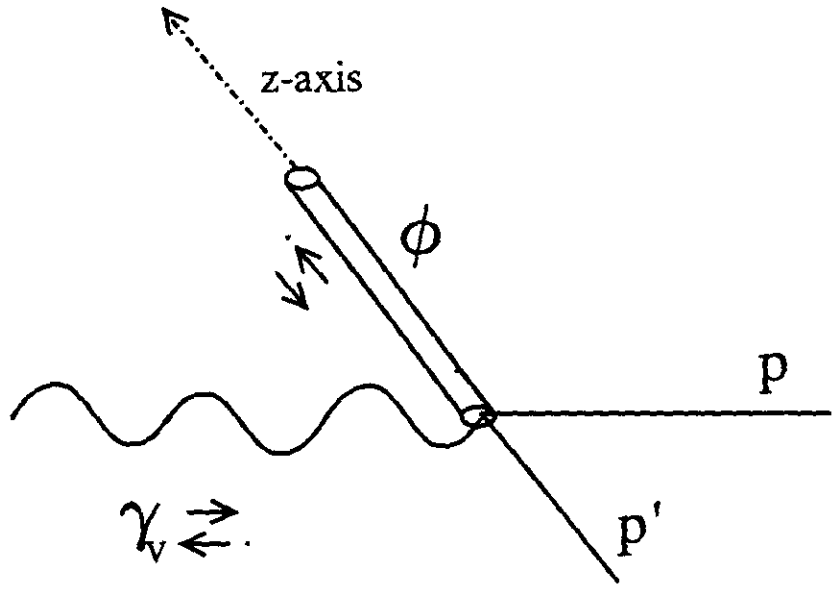


b) **Helicity Frame** (Hadronic c.m.)

**Figure 20** Definitions of a) the Gottfried-Jackson and b) the Helicity frames. Note that in both cases the angular distributions are measured in the $\phi$ rest frame.